FATIGUE OF CARBON NANOTUBE-LOADED POLYACRYLONITRILE FIBERS

A THESIS
PRESENTED TO
THE ACADEMIC FACULTY
BY

VINCENT WU

IN PARTIAL FULFILLMENT
OF THE REQUIREMENTS FOR THE DEGREE
MASTER OF SCIENCE IN MATERIALS SCIENCE AND ENGINEERING

GEORGIA INSTITUTE OF TECHNOLOGY

MAY, 2015

FATIGUE OF CARBON NANOTUBE-LOADED POLYACRYLONITRILE FIBERS

APPROVED BY:

DR. CHRISTOPHER L. MUHLSTEIN
COLLEGE OF ENGINEERING
Georgia Institute of Technology

DR. SATISH KUMAR
COLLEGE OF ENGINEERING
Georgia Institute of Technology

DR. MEISHA SHOFNER
COLLEGE OF ENGINEERING
Georgia Institute of Technology

DATE APPROVED: DECEMBER 11, 2014

Acknowledgments

The author gratefully acknowledges the Muhlstein research group for their help and support: Chris Muhlstein, James Collins, Wade Lanning, and Yoon Joo Na. He also thanks the Kumar research group members for providing insight into loaded fiber fabrication.

Table of Contents

List of Tables

List of Figures

List of Symbols

A = area (m^2)

d = diameter (μm)

σ_f = fracture stress (MPa)

F = force (N)

δ = displacement (mm)

$\Delta\sigma$ = stress range (MPa)

t_f = experimental creep lifetime (sec)

B = material-specific constant

n = material-specific constant

σ_c = reference strength (taken as average tensile strength, MPa)

t_{fc} = pure cyclic lifetime (sec)

σ_m = stress midway between the mean and amplitude stresses (MPa)

l = whole number index from 0 to $n/2$ rounded up to the nearest whole number

Summary

The effects of loading polyacrylonitrile (PAN) single fibers with carbon nanotubes (CNTs) on mechanical damage accumulation processes are explored in this thesis. Tensile, fatigue, and creep experiments were conducted to establish the effects of CNTs on the strength, fatigue lifetime, and viscoelastic/plastic (creep) damage accumulation. Three different configurations were tested: neat PAN fibers, PAN fibers loaded with multi-walled CNTs (MWCNTs) in the core, and PAN fibers loaded with few-walled CNTs (FWCNTs) uniformly throughout. The tensile results yielded load and displacement data from which failure stress was determined for all three fiber groups. During stress-life fatigue tests (runout lives 600,000 cycles) the fibers displayed similar fatigue susceptibilities, but in static load creep tests, the different fiber configurations led to a wider range of responses. The different fiber processing parameters used for each fiber group lead to a variety of viscoelastic and viscoplastic properties within each system, resulting in a range of damage accumulation mechanisms.

Keywords fatigue, creep, polyacrylonitrile, fibers

1 Introduction

Polyacrylonitrile (PAN) is an acrylic polymer whose electrical, thermal, and mechanical properties can be modified via loading with carbon nanotubes (CNTs).[1] How these properties change depends upon various factors such as nanotube type (e.g. single-walled or multi-walled), weight percent, and spatial distribution. The present study compares tensile, fatigue, and creep behavior of loaded and unloaded fibers and observes the effect of CNT loading on the fibers' properties.

PAN polymer is formed from acrylonitrile, a monomer with the general formula C_3H_3N. (Figure 1.1) The monomer is not symmetric, and thus PAN is not a symmetric polymer. The presence of nitrile and hydrogen groups along the carbon backbone means that PAN can form isotactic (consecutive monomers aligned the same way), syndiotactic (consecutive monomers regularly alternate in alignment), or atactic (monomers randomly aligned) configurations. The degree of crystallinity in the polymer is affected by the degree to which the PAN takes on each of those configurations. However, the strongly polar nitrile groups on each of the PAN chains prevent the polymer from being fully amorphous, and repulsion between the nitrile groups on the same chain usually contorts it into an irregular helix.[2] For the majority of commercial applications, acrylic polymers such as PAN feature a number average molecular weight in the range of 40,000-70,000 g/mol and a weight average molecular weight in the range of 90,000-170,000 g/mol.[2] They are produced via one of a variety of polymerization processes, a commonly utilized method being solution polymerization, where monomers are immersed in a suitable solvent and linked into polymer chains.[2] Other possible methods include aqueous dispersion, emulsion, and bulk polymerization. [2] Once formed, the PAN fiber is extracted by either wet spinning, in which the solvent is replaced by non-solvent that is then washed away, or dry spinning, in which solvent is evaporated with heated air.[2]

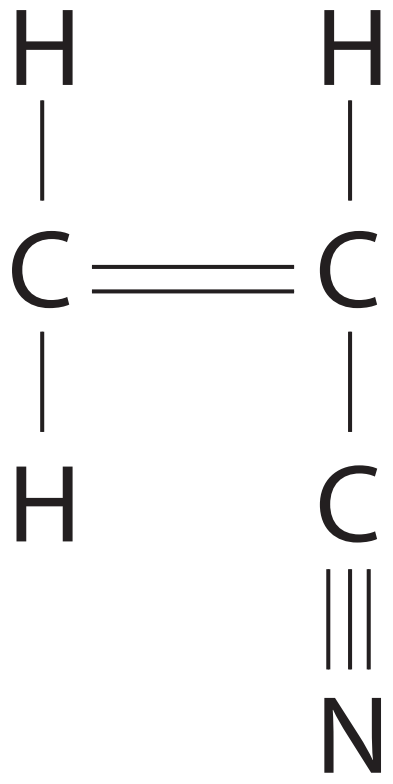

Figure 1.1: The acrylonitrile monomer.

Fabrication of CNT-loaded PAN involves a variation of wet spinning called dry-jet wet spinning. In this process, PAN and CNT powders are dissolved in an appropriate solvent such as dimethylformamide or dimethyl acetamide, with solvent added or evaporated intermittently throughout the process to achieve targeted concentrations. The solution is then spun into an air gap of established length before solidifying in coagulation baths. Finally, the solidifying material is drawn into fibers in the drawing bath and subjected to heat to evaporate any excess solvent.[1, 3] Chae et al. evaluated the mechanical behavior of this composite material for various nanotube configurations, including single-walled, double-walled, and multi-walled. For the multi-walled configuration, Chae found an elastic modulus of 10.8 GPa, a breaking strength of 412 MPa, and a strain to failure of 11.4% for bundles of at least ten filaments. These quantities show significant improvement over plain PAN fibers (7.8 GPa, 244 MPa, 5.5 %).[3] The fibers received for this study specifically were fabricated via a gel.[4]

1.1 Fatigue Behavior of Polymeric Solids

A great deal of literature is available regarding the fatigue mechanisms of solids. Like all polymers, PAN is composed of long molecular chains, and this combined with the previously mentioned side groups prevents PAN from being fully crystalline like most structural metallic alloys. It must further be noted that studies typically emphasize bulk polymer specimens rather than individual fibers. However, there are still many important fatigue deformation and crack growth details to take away from the work done on bulk polymer materials.

Like crystalline materials, polymer fatigue occurs due to the kinematic irreversibility that results from certain microscopic deformations.[5] The two mechanisms most commonly responsible for producing this damage in polymer materials are crazing and shear flow. A craze forms under tensile loading conditions in an orientation normal to the direction of the applied stress and is characterized by fibrils of polymer molecules that span across the craze and are interspersed with regions of porosity.[5] Meanwhile, shear flow leads to the formation of shear bands oriented in the direction of the largest shear stress. The beginning of yielding in a polymer is characterized by the appearance of shear bands.[5]

An area where polymer and metal behavior diverge regarding fatigue is in the actual deformation behavior. For example, while metals can experience either cyclic softening or cyclic hardening under fatigue conditions, polymers usually exhibit cyclic softening behavior.[5] Second, polymers respond much more strongly to significant thermal effects as a result of high strain rates, leading to situations of reduced fatigue life. Finally, the form of fatigue deformation in polymers, due to the presence of long molecular chains with assorted functional groups, is much less straightforward than in metals, which experience repeated dislocation glide.[5] Polymers can deform via a variety of mechanisms, such as chains straightening out and disentangling and functional groups changing orientation.

Many influences contribute to a material's fatigue life, but a prevailing factor that influences the fatigue life of polymers is the stress amplitude. This effect can be represented by a standard Wöhler curve that plots stress against number of cycles to failure on a semilog graph (i.e. an S-

N curve). The curve can be divided into three regions that separately describe the influence of stress on the total cycles to failure in the context of crack formation and growth due to crazing. Such fatigue crack growth can progress in different ways through a polymer, with distinct surface features accompanying each form. Small increases in crack growth rate per cycle produce fatigue striations whose spacings correspond to these individual increases.[5] Discontinuous growth bands, on the other hand, are indicative of relatively large jumps in crack growth and tend to be spaced much further apart than fatigue striations, implying advance of the crack only after every few hundred cycles. In addition to these crazing-induced surface features, a combination of crazing and shear flow can result in epsilon discontinuous crack growth, appropriately named as the features which form are shaped like the symbol ε.

Other important factors can affect fatigue life as well. These include high frequency testing (i.e. higher than 10 Hz), which often results in shorter fatigue life due to hysteretic heating softening the material, and specimen dimensions, in which thinner specimens disperse that heat to the environment more effectively and thicker specimens less so. Of course, environmental factors such as aggressive chemicals can shorter fatigue lives as well. Finally, higher molecular weight polymers tend to show increased resistance to fatigue crack growth, resulting in longer fatigue lifetimes than those with lower molecular weights.[5]

Fatigue behavior of polymer matrix composites has also been explored with various forms of reinforcing material. As one example, short, discontinuous inclusions of glass or carbon fibers loaded into a polysulfone matrix increase the fatigue life of the composite by lowering the strain experienced per cycle for a set stress level. Carbon fibers, with their higher stiffness, provided superior benefit compared to the glass fibers, and both displayed improvement over the plain polymer matrix. Another experiment with glass fibers in polyethersulfone showed that the inclusions improved the material's crack growth resistance as well.[5]

1.2 Single Fiber Testing of Neat Fibers

Testing of single acrylic fibers like polyacrylonitrile, and single fiber synthetic polymers in general, has been explored extensively in the 1960s and 1970s by Bunsell and Hearle.[6, 7, 8] Up to that point, single fiber tensile fatigue testing produced somewhat ambiguous results due to the inelastic response of many test specimens, which produced slack as the specimens endured repeated cycles of tension. If a constant extension was applied to a specimen, eventually the slack would be such that the specimen no longer experienced any stress. If a cumulative extension was applied, slack would be removed, but the imposed strain would gradually build to the point that it would be unclear if fiber failure occurred due to fatigue or simply creep. Thus, Bunsell and Hearle introduced a tensile fatigue setup that stressed the fibers via force-controlled tests, thereby insuring that the maximum load was kept constant. Using this apparatus, Bunsell and Hearle were able to differentiate between experiments that failed due to creep and those that ended due to fatigue. As such, they were able to go a step further and examine ruptured fibers using a scanning electron microscope to determine any differences in the failure mechanisms. Their early efforts with polyester, polyamide, and polyacrylontrile fibers revealed that distinct processes characterized creep and fatigue failures. Acrylic fibers, for example, exhibited a granular fracture surface after breaking due to creep, while a fatigue failure was characterized instead by axial splitting.[7, 8]

Since then, there have been many single fiber mechanical behavior studies of various other polymers evaluating tensile, fatigue, and creep responses. Those that specifically followed the setup established by Bunsell and Hearle includes Bencomo-Cisneros et al.[9], Harzallah et al.[10], and Davies et al.[11], who evaluated the tensile behavior of Kevlar-29, cotton, and poly(p-phenylene benzobisoxazole), respectively. Harzallah and Davies also evaluated the fatigue behavior of their respective fibers, and all three followed the example of Bunsell and Hearle in supplementing their results with fractography images of their fibers' fracture surfaces, extracting specific information on their failure mechanisms. For example, Bencomo-Cisneros's and Harzallah's electron micrograph images showed strong indications of axial splitting in their respective fracture surfaces. There have been studies published on the creep behavior of polymer fibers, with Lechat et

al.[12] contributing to the small body of work with creep testing of polyethylene terephthalate and polyethylene naphthalate.

1.3 Single Fiber Testing of Loaded Fibers

To add to the single fiber literature, many studies have loaded fibers with various reinforcing materials in an attempt to improve the fibers' properties. Mahfuz et al.[13] explored the strength and elastic modulus of Nylon 6 fibers loaded with MWNTs and found that the loaded nanotubes improved both properties markedly. Moore et al.[14] did the same with SWNTs loaded into polypropylene fibers, although the effect of the nanotubes proved to vary depending on certain processing parameters of the initial polypropylene. Rangiri et al.[15, 16] worked with both polymers, loading instead with silicon nitride nanorods and nanospheres, and observed improvements in strength and modulus. Mahfuz and Rangiri both attributed the improvements to successful alignment of the tubes/rods along the direction of the fibers, enabling the reinforcing material to contribute its strength properties to the polymer in the composite fiber. However, there is less research available on what changes loaded polymer fibers experience with regards to their fatigue and creep behavior.

This thesis will take a series of PAN-based single fibers and explore their fatigue-creep damage accumulation mechanisms, including how they are influenced by the configurations' different processing histories and final morphologies. While it is tempting to assume that the cyclic and creep behavior would resemble that of single fiber PAN, the loading of the CNTs changes the local structure of the fiber[1, 3], so expecting similar responses between loaded and unloaded fibers may be unfounded. The remainder of this thesis, broken up into chapters, will explore this question more fully. Chapter 2 will detail the materials and methods used in the study, including specimen preparation, mechanical tests, and data acquisition and analysis procedures. Chapter 3 will study the results, experienced in both graphical and tabular form, and explore the implications of observed trends. Finally, Chapter 4 will summarize the findings and offer suggestions for follow-up work.

2 Materials and Methods

This chapter describes the materials and methods used to test single PAN fiber and CNT-loaded fibers and to observe the range of damage accumulation mechanisms in fibers. The first section will detail the as-received properties of the fibers at the center of the study. Next, the preparation of specimens is described along with earlier iterations of the process that proved less successful. The section following outlines the mechanical testing equipment and procedures used to determine the tensile, fatigue, and creep properties of the specimens. Finally, the last section provides the equipment and procedures utilized in imaging the fracture surfaces of the specimens post-failure.

2.1 Material Specifications

The material under investigation was three configurations of microfilament polyacrylonitrile (PAN) fibers. The first configuration was neat PAN fibers (Figure 2.1). The second was PAN fibers loaded with multi-walled carbon nanotubes (MWNTs) in the core of the fiber, leaving the shell free of MWNTs (Figure 2.2). These two configurations were delivered as discrete fibers. The third configuration was PAN fibers loaded with few-walled carbon nanotubes (FWNTs) uniformly distributed throughout the fiber (Figure 2.3) and was delivered as a bundle. The neat fibers had a nominal diameter of 16.0 μm and a designation of NF. The core-shell fibers had a nominal diameter of 16.0 μm and a designation of CS. The uniformly loaded fibers had a nominal diameter of 11.1 μm and a designation of UL.

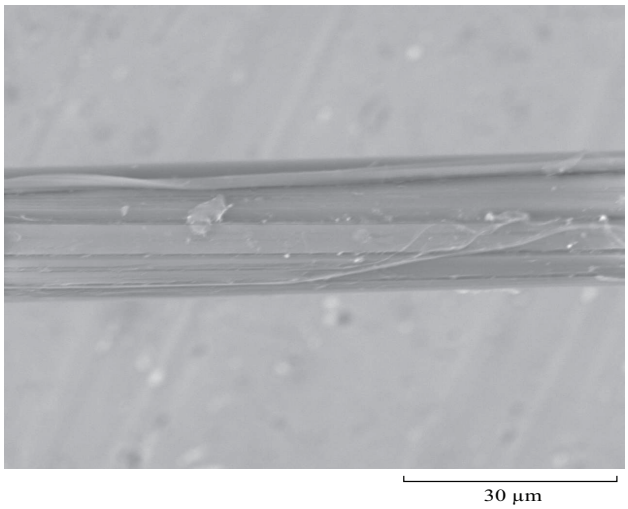

Figure 2.1: Scanning electron micrograph of the surface of a neat fiber.

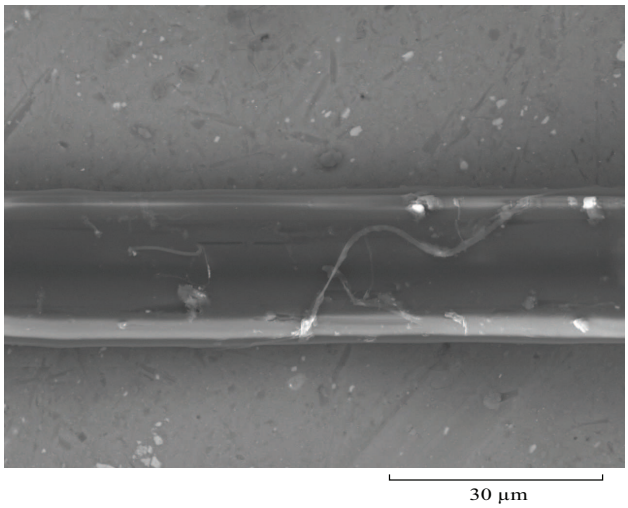

Figure 2.2: Scanning electron micrograph of the surface of a core-shell fiber.

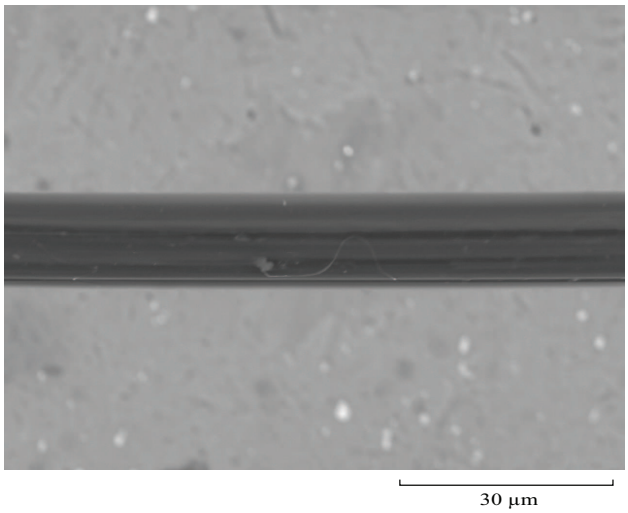

Figure 2.3: Scanning electron micrograph of the surface of a uniformly loaded fiber.

Over the course of this thesis, it will be assumed that the fibers feature circular cross-sections in order to simplify stress calculations. Obviously, there are limitations to this approximation, as it is likely that the fibers are not radially symmetric and the resultant calculated stresses are thus affected significantly. The approximation is used merely as an initial approach to quantifying the mechanical properties of the fibers.

2.2 Single Fiber Sample Preparation

In the testing of single fiber polymers, the most effective method of mounting them in the testing apparatus proved to be attaching them first to paper tabs. These paper tabs were cut as 190.05 mm$\times$12.70 mm rectangles from notebook grid paper featuring 6.35 mm$\times$6.35 mm squares (corresponding to 0.25 in$\times$0.25 in squares). A strip of double-sided tape was placed on one edge of one side of each tab, covering an area 12.70 mm$\times$6.35 mm (i.e. the two squares at the end of each tab). The tabs were then placed, tape side up, on a glass slide marked with 6.35 mm increments and oriented such that the taped edges were aligned outwards. This setup was subsequently placed on top of a fluorescent light.

A length of single fiber 2 to 8 cm long was teased with metal tweezers out of the bundle or

spool in which it was provided and snipped off with scissors. It was then stuck to the taped ends of the paper tabs, one fiber end per tab, such that when the entire specimens was gently pulled taut, the fiber straightened and remained secured to the paper tabs. Throughout this sticking process, the grids on the tabs and the marked slide underneath were used to center the fiber relative to the tabs and establish a gap of 6.35 mm between the inner (untaped) edges of the tabs. (Figure 2.4.) The backlighting provided by the fluorescent light made seeing the single fiber easier, particularly in the case of the extremely fine, neat fiber.

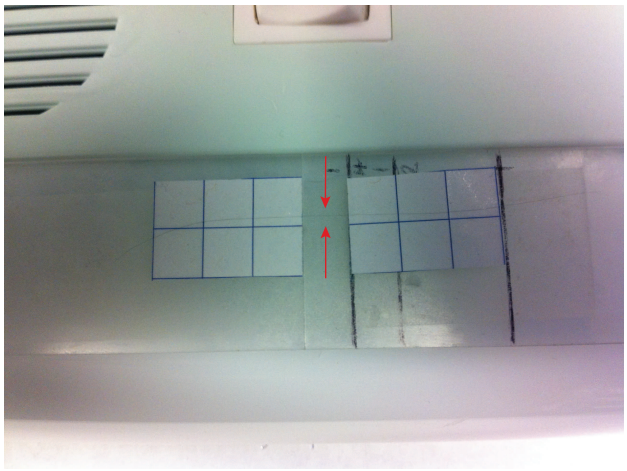

Figure 2.4: Placing the fiber (located between the red arrows) onto the paper tabs. The fiber is secured to the tabs via strips of tape on the two outermost squares of each tab. Each box is 6.35 mm(0.25 in) in width.

Once the specimen was pulled taut, a drop of Norland Optical Adhesive Ultraviolet Curing glue was applied to one paper tab such that the center of the drop was approximately 6.35 mm from the inner edge of the tab and 6.35 mm from each long edge. (Figure 2.5) Tweezers were used to gently press down on the section of the fiber submerged by this drop to ensure it remained as flush against the paper as possible. The glass slide, with the specimen on top, was then placed on a tabletop between two small pieces of cardboard and covered with a third piece of cardboard such that the covering piece was supported by the other two pieces and did not contact the specimen at any point. The top piece covered the entire specimen except the last 12.70 mm of the paper tab with the glue.

As Figure 2.6 shows, the inner row of squares of the tab with the glue was covered, but the middle row and taped row was exposed. With the majority of the specimen shielded as such, UV light from an ELC-410 Light Curing System (Electro-Lite Corporation) was applied to the exposed part of the glue for at least 30 s. to cure it. Previously, a folded piece of plain paper was used to shield the specimen, but it proved inadequate for blocking UV light. A drop of glue was then applied in the same manner to the other paper tab and the process repeated, resulting in a specimen with a gage length of 19.05 mm (the sum of the inner square of one tab, the gap between the tabs, and the inner square of the other tab) between the cured glue grips. Uncured glue at the inner edges of each tab provided evidence that UV light was not applied to those regions, ensuring that no section of PAN fiber within the gage length was exposed to damaging UV radiation. (Figure 2.7.) While the ideal situation would have involved curing the entire droplet of glue used and measuring the gage length from the tips of solidified glue, it was too difficult to reliably construct samples in this way without exposing sections of fiber near the grips to UV light. Indeed, early attempts at sample preparation in this manner resulted in a disproportionate amount of grip failures. The compromise was to construct samples in the manner described, using uncured glue as evidence that the gage length remained unexposed to UV light, and testing the samples immediately after preparation, assuming that the uncured glue did not contribute to gripping the fiber.

The final, complete configuration enabled the specimen to be loaded into the testing apparatus via the paper mounting tabs such that the gage length was axially aligned along the direction of action, as called for in ASTM C1557, which describes the tensile testing of single polymeric fibers. A previous iteration of the specimen preparation strategy involved attaching the fibers to tapestry needles instead of paper tabs, but in many cases, it was too difficult to see the fiber well enough to position it for proper curing. The small area also made it difficult to apply enough glue, whether by dropping glue onto the needle or by dipping the needle tip into the glue itself.

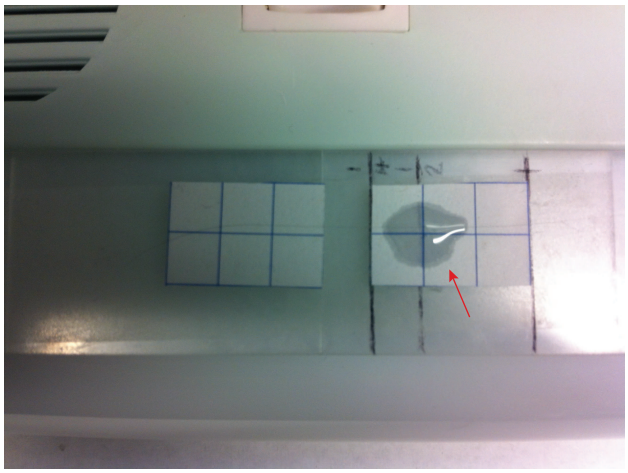

Figure 2.5: Applying the UV glue (red arrow). The center of the drop was roughly aligned with assistance from the grid lines on the tabs. One square was 6.35 mm (0.25 in) wide.

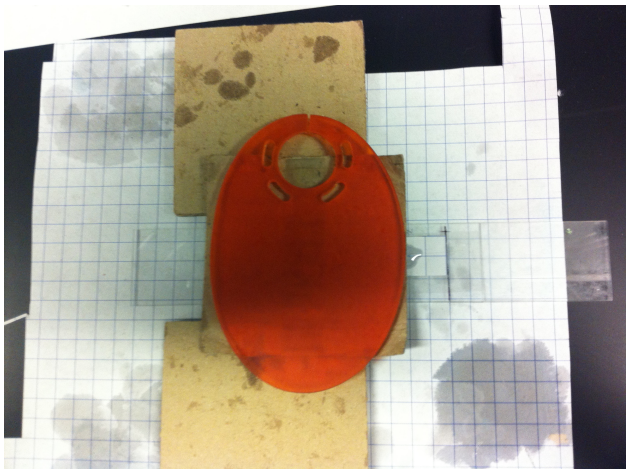

Figure 2.6: Curing the UV glue. The top cardboard piece, out of personal preference, was also weighed down with a taped piece of plastic for easier handling. The inner part of the fiber was shielded in this way so that no section of polymer within the eventual gage length was exposed to UV radiation. One square was 6.35 mm (0.25 in) wide.

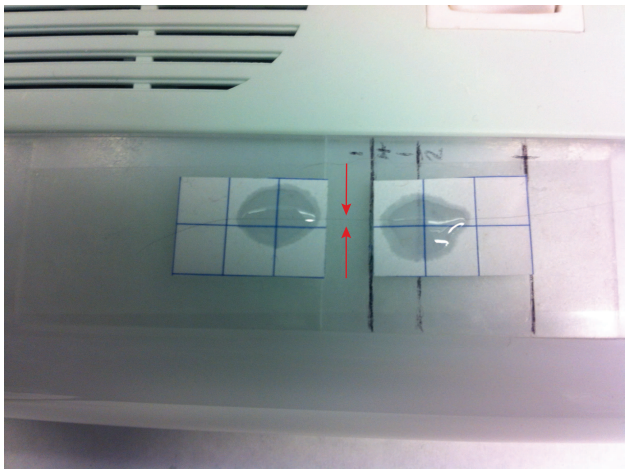

Figure 2.7: The completed specimen (with the fiber between the red arrows). One square was 6.35 mm (0.25 in) wide.

2.3 Mechanical Testing

Tensile, fatigue, and creep tests were carried out in ambient laboratory air using an Instron 5848 (Canton, Massachusetts, USA) microtester electromechanical load frame controlled by custom LabView software. The load cell was a Transducer Technique GSO-250 (Rio Nedo Temecula, California, USA) with a resolution of 0.1% of full scale ($\pm$ 250 grams). Proportional-integral-derivative (PID) tuning of the load frame was performed as described by the load frame instruction manual for force-controlled tests. The parameters that produced the best results for both loaded fibers were a proportional in the range of 31.00-35.00 dB, an integral of 1.60 I/sec, a derivative of 0.00 msec, and a lag of 23.50 msec. For the neat fibers, proportional was 28.00 dB, integral was 0.40 I/sec, derivative was 0.00 msec, and lag was 18.00 msec.

Spring-loaded vise grips were used to grip the top and bottom of the specimen at the paper tabs. The grips were kept in the same alignment in which they were used to perform the PID tuning, as the orientation of the grips had a noticeable effect on the values of the ideal parameters. This was likely due to a slight difference in how the system flexed when the grips were aligned in a different configuration. Other grips experimented with in this setup included pneumatic and fiber grips. Electrical connection problems with the pneumatic grips prompted a change to a manually

controlled method. It was believed that the fiber grips would simplify specimen preparation by allowing the single fibers to be looped directly into the grips, which would then be tightened securely. However, the fineness of the fibers made it difficult to see and recover the pieces post-failure, so a switch was made to the spring-loaded vice grips, into which loading the paper tabs proved simple.

The Instron load frame and camera setup were positioned on an aluminum plate placed on top of a Minus-K (Inglewood, California, USA) model 250BM-1C 265 lb capacity vibration isolation system with model 350 BM-1 horizontal stiffening columns. In order to shield the setup from air currents flowing around the lab, an enclosure was constructed out of 80/20 aluminum and polycarbonate sheets. The frame took the shape of an upright rectangular prism on wheels, and polycarbonate sheets were installed on all four sides as well as the top. The front panel was removed whenever a new experiment was being set up and replaced just before the test was started. The enclosure was constructed after most of the tensile tests had already been completed, so those tests were conducted in completely open air.

The specimen was secured into the Instron via the top grip first and left hanging freely, making as little contact, if any, with the bottom grip as possible. Next, the load cell was tared, the pins removed, and the specimen lowered so that the bottom tab could be secured into the bottom grip. After setting the "specimen protect" function, a preload was applied to the fibers prior to beginning the test.

2.3.1 Tensile Tests

Ten single fibers from each group were prepared to produce results. Each tensile test was displacement-controlled and set with a ramp amplitude of 10.00 mm and a ramp rate of 1.00 mm/min. After appropriate position and load limits were set to prevent cross-head displacement beyond the desired range, the mechanical test was started, and the fiber was extended until fracture, with 50 position and load values recorded every second. The ramp amplitude and rate resulted in a tensile frature under 30 s. for every test, as required by ASTM C1557.

2.3.2 Fatigue Tests

Six to nine specimens per condition were fatigue tested under force-controlled loading conditions and set with a haversine waveform, a frequency of 1 Hz, appropriate position and load limits, and a cycle limit of 1,000,000. Tests were designed to run until fracture, but if none occurred after about 600,000 cycles (roughly seven days), the test was considered a runout and manually stopped. The fibers were tested at different, targeted stresses by considering the diameter as previously found for each fiber and defining the amplitude and mean stresses accordingly, maintaining a load ratio of 0.1. There is no specific ASTM standard that addresses the cyclic fatigue testing of single polymeric fibers. Some guidance was thus drawn from ASTM D7774, which outlines the standards of flexural fatigue testing of plastics. In particular, this standard recommends a test frequency less than 5 Hz, making the current use of a 1 Hz frequency a reasonable decision.

2.3.3 Creep Tests

Three to seven specimens per condition were subjected to sustained load creep tests. Each creep test was force-controlled and set with a trapezoidal ramp. The first stage of the test, the ramp up to the target amplitude, was set to a rate of 0.5 N/min. The second stage, the hold, was set to the target amplitude and programmed to last for 10,000 min. The final stage of the test, the ramp back down, was also set to a rate of 0.5 N/min. Proper position and load limits were set as well.

The fibers were each tested at various percentages of their respective mean fracture strengths as measured from the tensile tests. Tests were designed to run until fracture or until 10,000 min. (600,000 s.) had passed. However, the Instron would usually continue to hold beyond the 10,000 min. limit if no break occurred, so runouts had to be manually stopped. There is no ASTM standard that specifically addresses static loading of single polymeric fibers, although guidance may be drawn from ASTM E139, which describes creep testing of metallic specimens.

2.3.4 Analysis Methods

Every test returned a text file detailing the position, time, cycle, and load at every 0.02 s. of the experiment from start to finish. Fracture stress was found by first converting the nominal, average diameter provided with the as-delivered fiber batches to meters and determining cross-sectional area A from it:

$$A = \frac{d^2 \times \pi}{4}, \tag{2.1}$$

where d is the diameter. Then, every recorded load value was divided by the area:

$$\sigma = \frac{F}{A}, \tag{2.2}$$

where σ is stress in MPa and F is load in N.

Force-displacement plots were generated using the raw load and position values, using the difference between each position value and the initial position to express crosshead displacement. Force and displacement were also each plotted against time in semilog plots, and in the case of the fatigue tests, stress levels were plotted against number of cycles to failure. With these data sets and plots, mechanical quantities were thus extracted or calculated. Failure stress was obtained using the final load recorded at the end of each tensile test, as it represents the load at which rupture occurred. Fatigue and creep lifetimes were equivalent to the duration of the corresponding tests until failure occurred. If no fracture event was observed after about seven days, the lifetime of the test was given as the amount of time elapsed at the point the test was ended, rounded to the nearest second.

2.4 Fracture Imaging

After completion of all mechanical tests, the fracture surfaces of the specimens were examined using a Hitachi TM3030 Tabletop SEM (Newport Beach, CA, USA). To prepare a specimen for viewing in the SEM, tape was used to capture a ruptured end such that the fracture surface stuck

out a few millimeters from the edge of the tape, with the majority of the fiber gage length adhered to the sticky tape surface. The rest of the specimen (i.e. the paper tab) was cut away and the tape folded over once or twice to secure the fiber end in place. To mount the fiber specimen into the SEM, a custom stub was designed out of aluminum rod stock (M4-0.7). Featuring an outer diameter of 14.5 mm and an inner diameter of 3.5 mm, a stub 3.5 mm in height was cut from the stock. A power drill was used to bore a small hole into the top of the stub, and a small washer and screw secured a small copper alligator clip in place. Once the setup was tested to ensure no part came loose, it was broken down into parts and washed manually with acetone, manually with isopropanol, ultrasonically with detergent, and once more manually with isopropanol. Once the specimen was secured into the alligator clip, the stub was screwed into the SEM and the fracture surface examined. Handling was restricted as much as possible to the aluminum stub, as too much handling of the alligator clip could jar it loose.

3 Results and Discussion

From the tensile, fatigue, and creep data acquired on both unloaded and CNT-loaded PAN fibers, quantities such as failure stress and lifetime may be determined. These properties help drive the examination of the damage accumulation processes occurring in each composite fiber system. In this section, the results of the tensile tests are provided first along with observations of the values obtained for failure stress. Next, the results of the fatigue tests, the amplitudes of which were percentages of the average tensile strengths, are provided along with discussions of the fibers' properties, including their respective lifetimes. Then, the results of the creep tests, the amplitudes of which were also based on the previously obtained tensile data, are presented to provide further information on fiber failure due to creep as opposed to fatigue. After a presentation of fractography, the chapter concludes with a closer look at the fatigue and creep life data to determine how viable a damage partitioning strategy is for characterizing the fatigue-creep coupling present in each fiber system.

3.1 Tensile Data

The results of the tensile experiments yielded force-displacement plots for all three fiber groups. A comparison of neat fiber specimens is provided by Figure 3.1. Failure stress averaged 591 ± 159 MPa. A representative plot of the neat fiber behavior is given by the stress-strain curve of NF_2T, shown by Figure 3.2. The fiber displays a typical elastic response until yielding roughly around a displacement of 0.2 mm and force of 0.055 N. It then experiences strain hardening until fracture. Cross-sectional reduction as a result of fiber elongation at no point overtakes the strain hardening effect, resulting in a monotonic increase in stress until rupture. The failure stress for this specific specimen was 584 MPa.

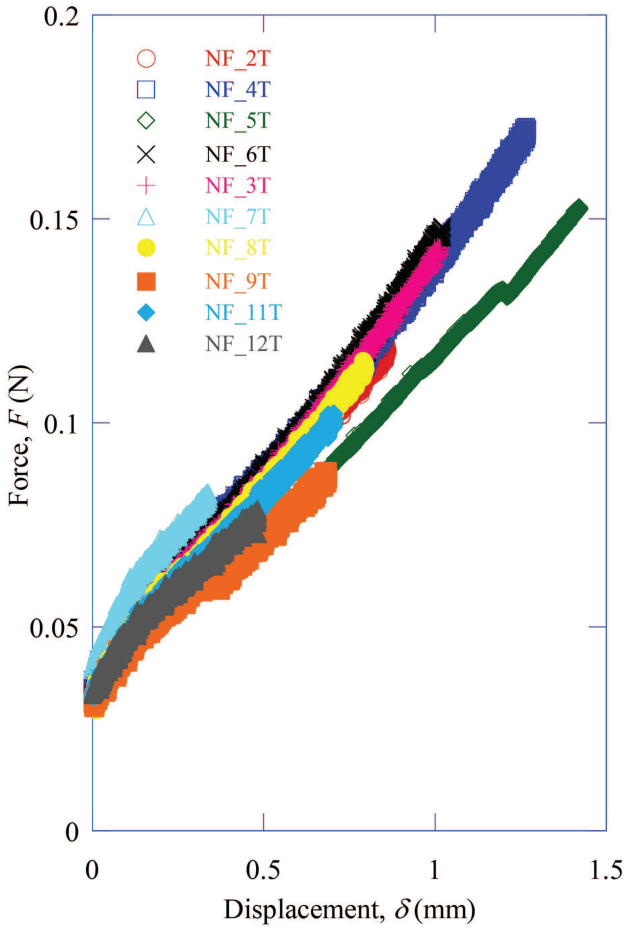

Figure 3.1: Force-displacement tensile plot for neat fibers. Failure stress averaged 591 $\pm$ 159 MPa.

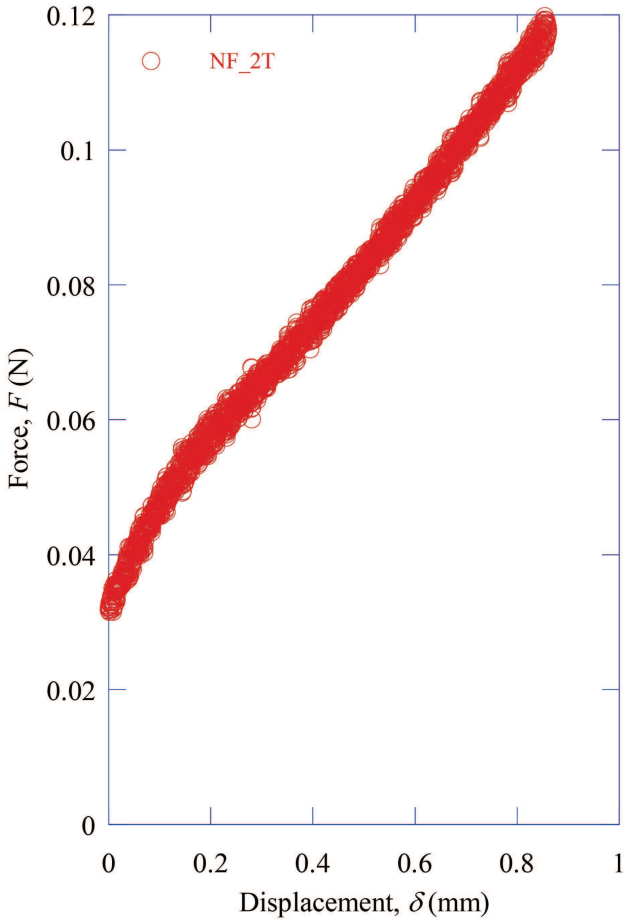

Figure 3.2: Force-displacement tensile plot for NF_2T. Failure stress was 584 MPa.

A comparison of core-shell fiber specimens is provided by Figure 3.3. Failure stress averaged 527 $\pm$ 125 MPa. A representative plot of the core-shell fiber behavior is given by the stress-strain curve of CS_3T, shown by Figure 3.4. Like the neat fiber, the core-shell fiber initially displays a typical elastic response, with yielding occurring at a displacement of about 0.15 mm and a force of about 0.055 N. It then also experiences strain hardening for the remainder of the test, showing a monotonic increase in stress until rupture. The failure stress for this specific specimen was 659 MPa.

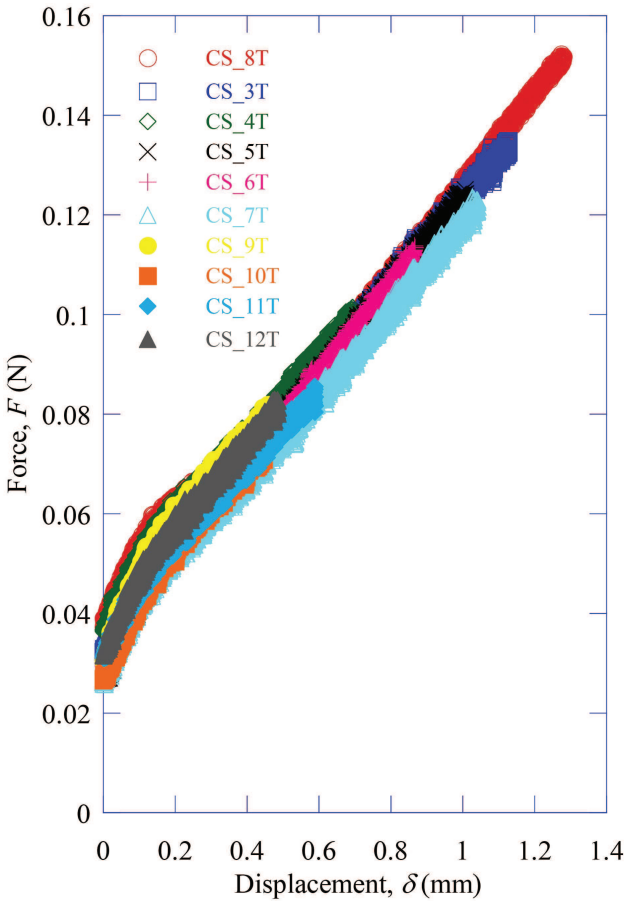

Figure 3.3: Force-displacement tensile plot for core-shell fibers. Failure stress averaged 527 $\pm$ 125 MPa.

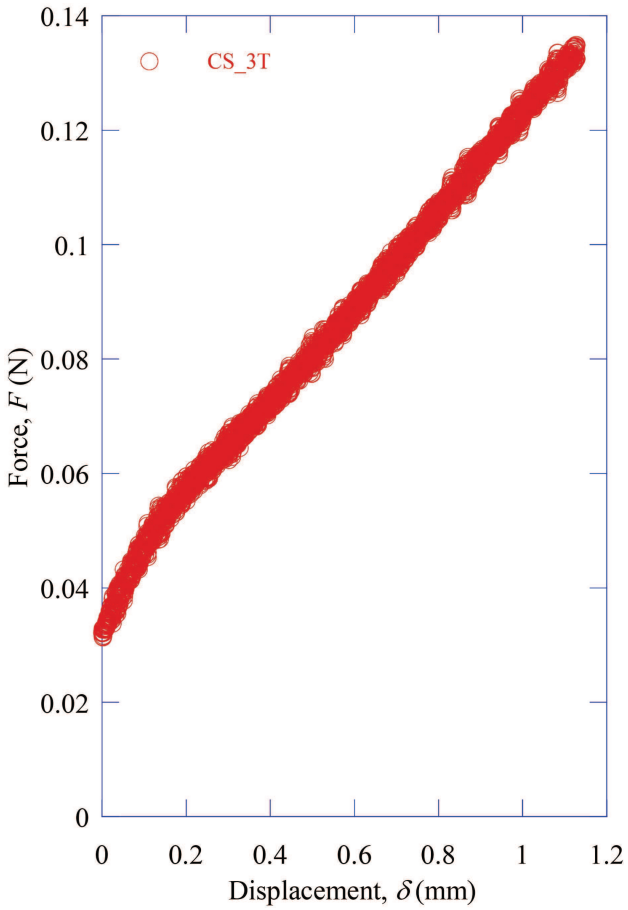

Figure 3.4: Force-displacement tensile plot for CS_3T. Failure stress was 659 MPa.

Finally, uniformly loaded fiber specimens are compared in Figure 3.5. Failure stress averaged 697 ± 186 MPa. A representative plot of the uniformly loaded fiber behavior is given by the force-displacement curve of UL_2T, shown by Figure 3.6. Featuring typical behavior similar to the other two fibers, yielding occurs at a displacement of around 0.2 mm and a force of about 0.015 N. The failure stress was 806 MPa.

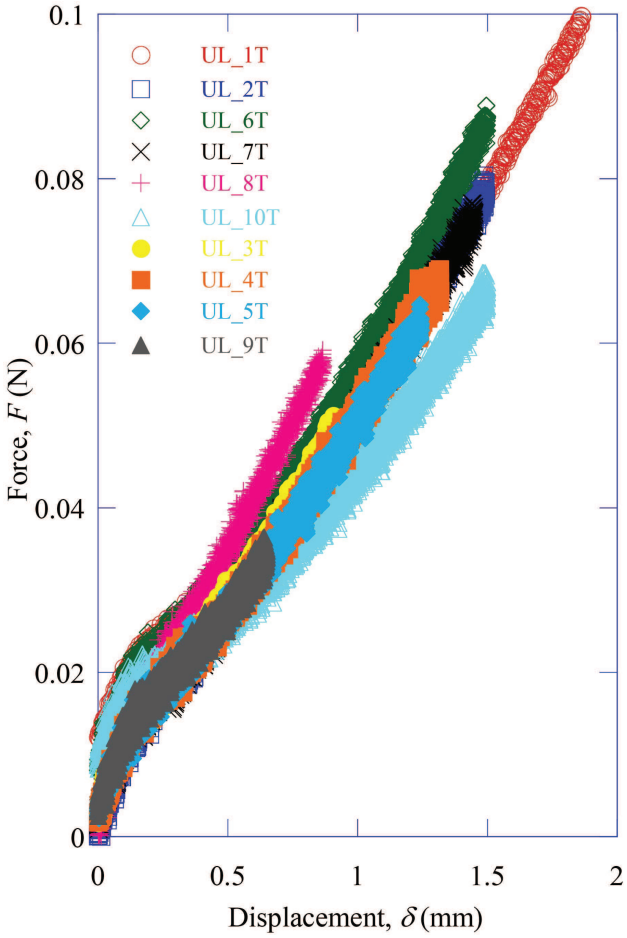

Figure 3.5: Force-displacement tensile plot for uniformly loaded fibers. Failure stress averaged 697 ± 186 MPa.

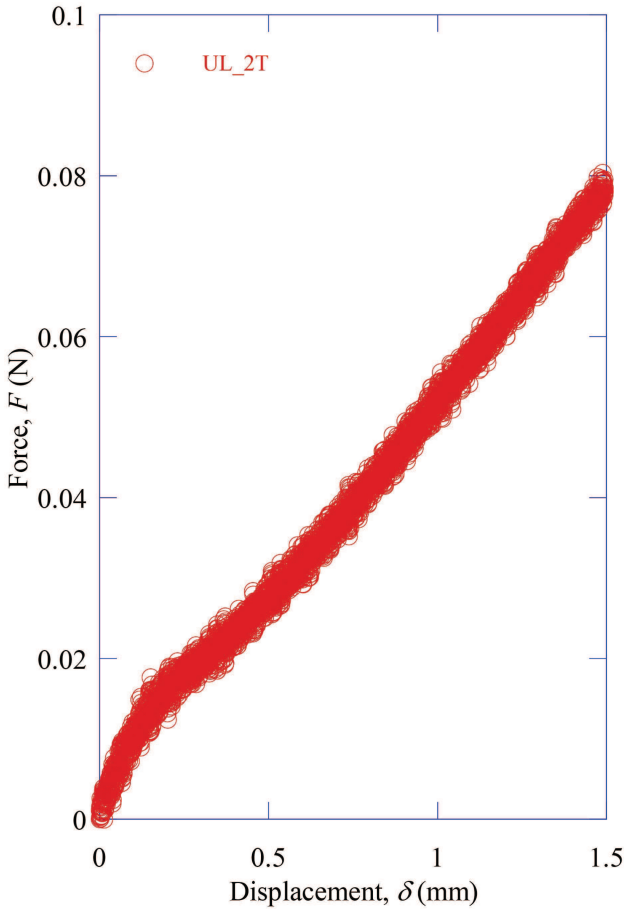

Figure 3.6: Force-displacement tensile plot for UL_2T. Failure stress was 643 MPa.

The full list of ultimate tensile strength values is given in Table 3.1. To reiterate, the abbreviation "NF" refers to the neat fibers, "CS" to the core-shell fibers, and "UL" to the uniformly loaded fibers.

Table 3.1: Ultimate strength of all tensile specimens.

Sample	Failure strength (MPa)
NF_2T	516
NF_3T	608
NF_4T	707
NF_5T	587
NF_6T	441
NF_7T	320
NF_8T	477
NF_9T	386
NF_11T	452
NF_12T	313
CS_3T	629
CS_4T	534
CS_5T	679
CS_6T	584
CS_7T	553
CS_8T	850
CS_9T	347
CS_10T	435
CS_11T	538
CS_12T	516
UL_1T	700
UL_2T	643
UL_3T	438
UL_4T	399
UL_5T	785
UL_6T	812
UL_7T	730
UL_8T	476
UL_9T	231
UL_10T	622

On their own, these data sets do not reveal much about the damage accumulation mechanisms occurring in the fibers. However, the fracture strengths do give a general idea of appropriate stress ranges to target in subsequent tests. With this information, cyclic load tests can be performed to study the fibers' fatigue lifetimes and observe the potential range in behavior due to the different fiber configurations and their respective processing histories.

3.2 Fatigue Data

The results of the fatigue data yielded cyclic stress-strain curves for all three fiber groups as well as stress-life curves to show the effect of stress level on total lifetime. The stress-strain curves for the three groups are given by Figure 3.7, Figure 3.8, and Figure 3.9. The core-shell and neat fibers show slow increases in strain that imply cyclic softening and a slow accumulation of damage as the fibers load and unload. The uniformly loaded fibers, on the other hand, tend to show a large shift in the strain early on before stabilizing, implying that a comparably larger amount of plastic strain occurs at the beginning of the fatigue process.

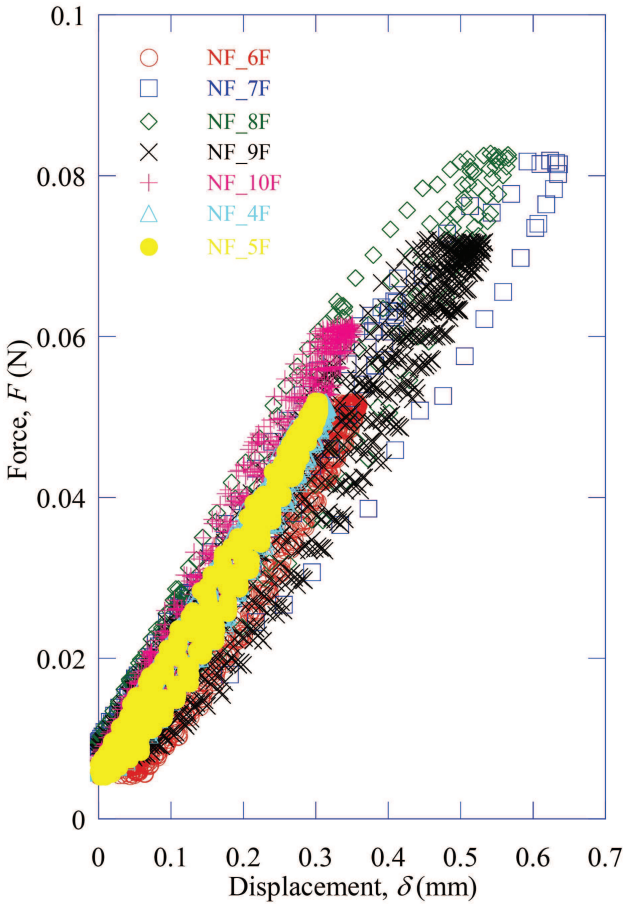

Figure 3.7: Cyclic force-displacement plot for neat fibers for the first 15 cycles. A relatively slow accumulation of damage is evident.

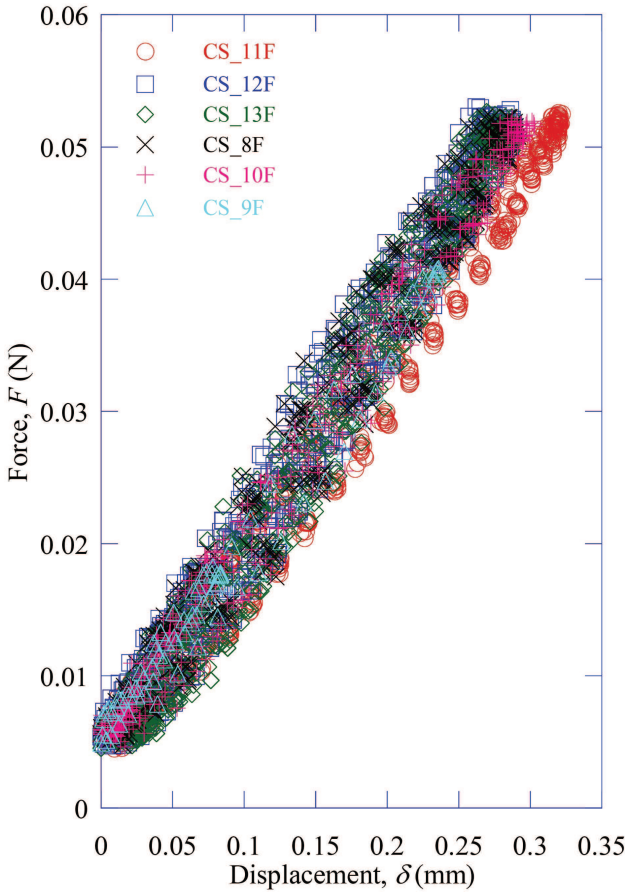

Figure 3.8: Cyclic force-displacement plot for core-shell fibers for the first 15 cycles. A relatively slow accumulation of damage is evident.

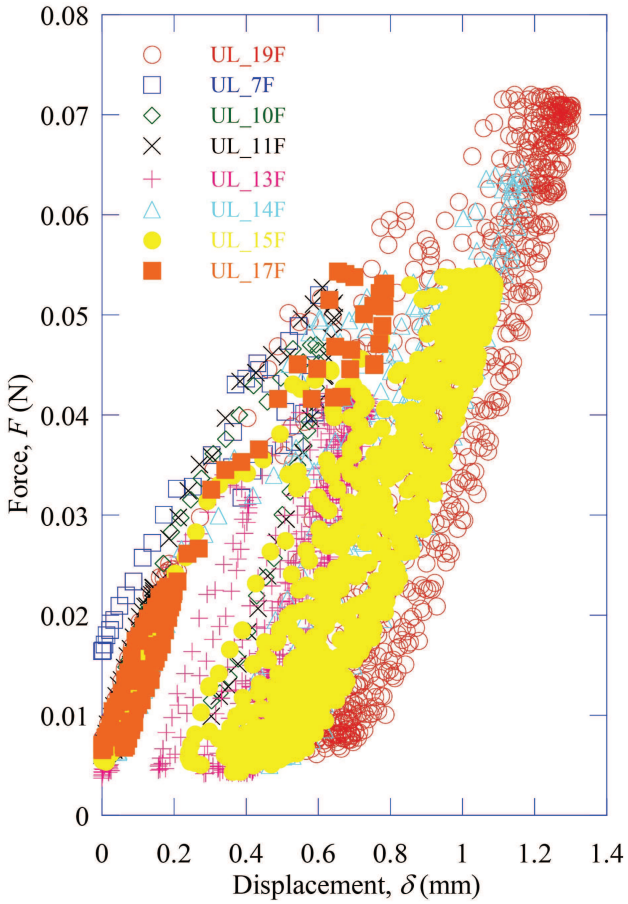

Figure 3.9: Cyclic force-displacement plot for uniformly loaded fibers for the first 15 cycles. Damage appears to accumulate more rapidly, resulting in greater increases in strain.

To check on the consistency of the experimental setup, displacement vs. time and force vs. time semilog plots were generated for each fiber group. The results show the fibers within each group displaying gradual increases in displacement as damage is accumulated and consistent force levels throughout the duration of their tests, implying reliable force control. Representative fiber data from each group are given in Figure 3.10 and Figure 3.11.

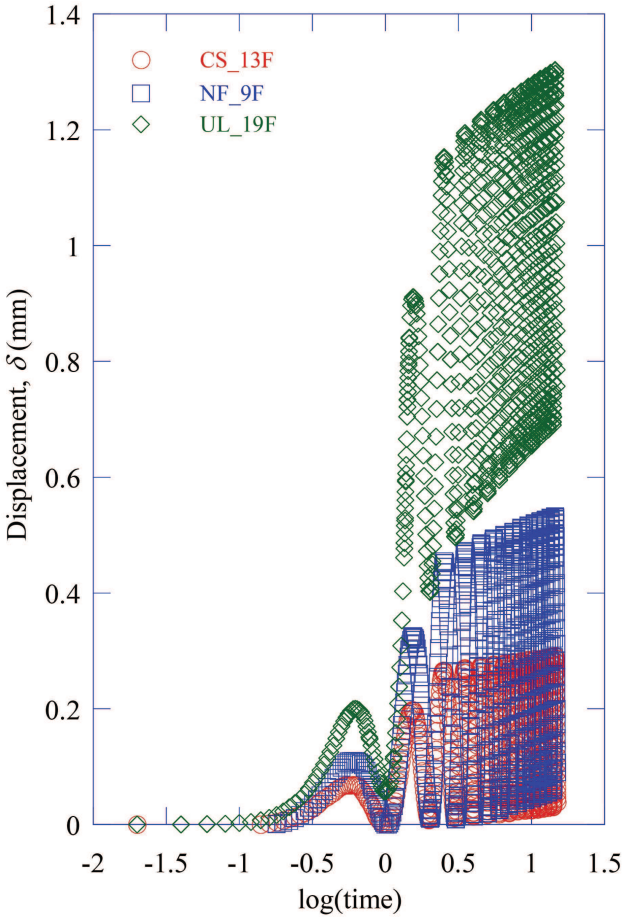

Figure 3.10: Displacement-time semilog plot for three different fibers for the first 15 cycles. The core-shell and neat fibers accumulated damage in similar fashion to each other while dissimilar in fashion to the uniformly loaded fibers.

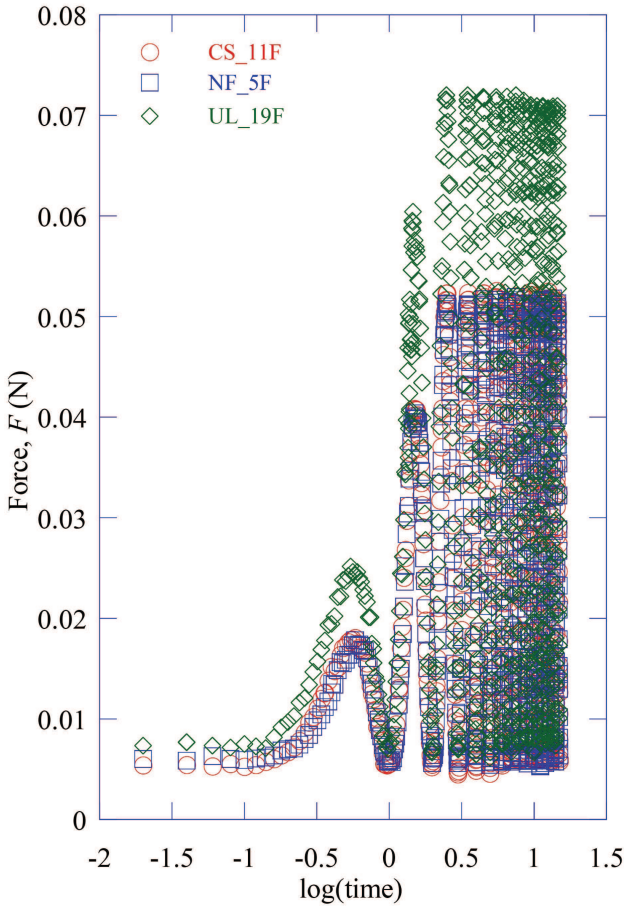

Figure 3.11: Force-time semilog plot for three different fibers for the first 15 cycles. Consistent force levels over time demonstrate satisfactory force control.

The stress range-life behavior of the fiber groups are given by Figure 3.12, and the results used to generate this figure are given in Table 3.2. The presence of multiple failures in each fiber group is indicative of a cyclic fatigue damage accumulation process occurring in the fiber systems.

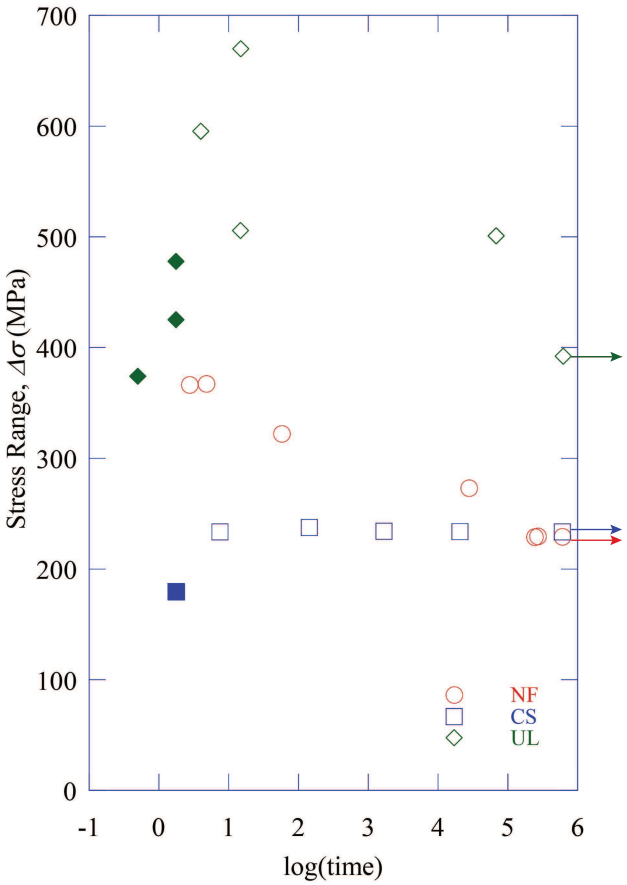

Figure 3.12: Stress range-life plot for the fibers undergoing fatigue tests. Filled-in symbols represent tests that broke in the initial envelope region of the test. Symbols with arrows extending to the right indicate run-out tests.

Table 3.2: Fatigue lifetimes of core-shell, neat, and uniformly loaded fiber specimens given various stress levels.

Sample	Stress Range (MPa)	Lifetime (cycles)
NF_4F	255	601002 (run-out)
NF_5F	255	267799
NF_6F	255	241139
NF_7F	407	3
NF_8F	408	5
NF_9F	358	58
NF_10F	304	27822
CS_8F	260	20538
CS_9F	203	2
CS_10F	260	8
CS_11F	260	1689
CS_12F	264	142
CS_13F	260	601230 (run-out)
UL_7F	537	1
UL_10F	486	2
UL_11F	545	2
UL_13F	436	619201 (run-out)
UL_14F	661	4
UL_15F	557	67635
UL_17F	562	15
UL_19F	744	15

While it is clear that the specimens experience cyclic fatigue damage, what it less clear is whether they are failing primarily due to cyclic fatigue effects or if there are other factors influencing their failure lifetimes. Specifically, it is possible that the fibers are suffering not only from fatigue, but from creep as well. Attempts to parse out the separate influences of fatigue and creep require data from static load creep tests, which will be presented in the next section.

3.3 Creep Data

The results of the creep data yielded stress-strain curves of the fiber groups that displayed the effects of creep and are given by Figure 3.13, Figure 3.14, and Figure 3.15. While the core-shell fibers showed clear susceptibility to creep, with specimens at various stress amplitudes all breaking

within a day, the neat fiber specimens all went for days without failing. The uniformly loaded fibers displayed a range of behavior varying from failure within tens of seconds to not breaking at all after over a week. The lifetimes of the specimens are given in Table 3.3, and it is clear from the data that these PAN fibers can show a range of susceptibility to creep ruptures.

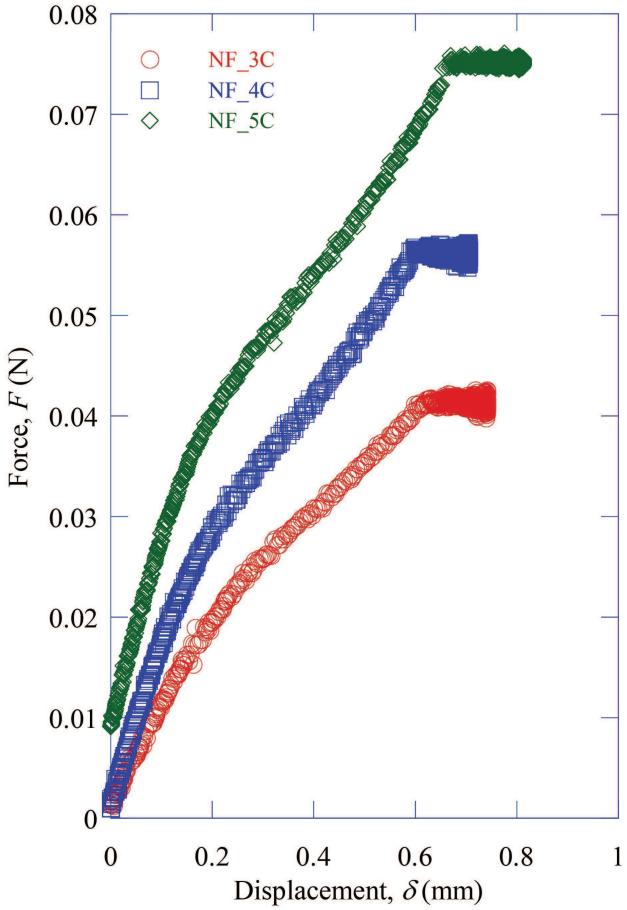

Figure 3.13: Force-displacement creep plot for neat fibers up to the first 60 s. of the test.

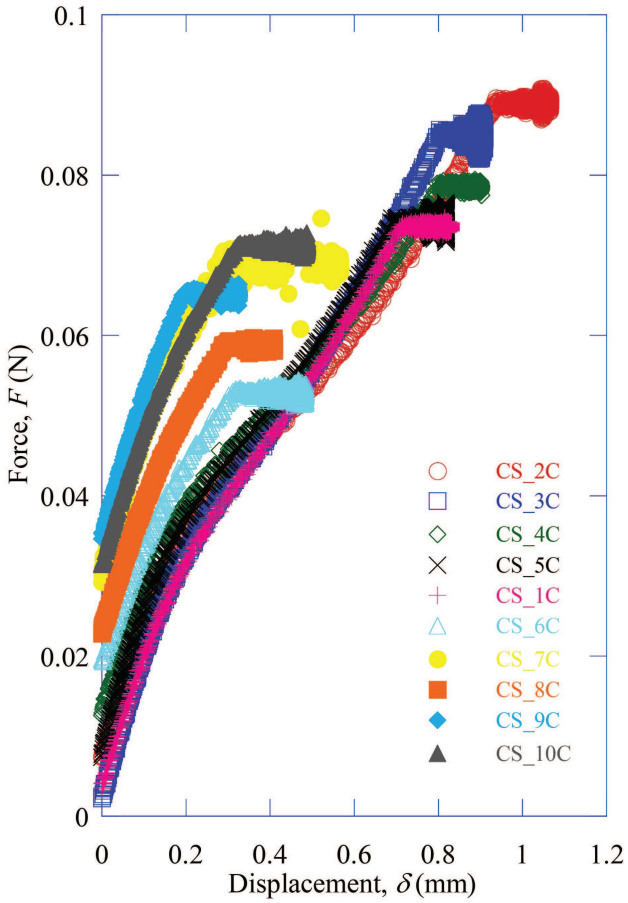

Figure 3.14: Force-displacement creep plot for core-shell fibers up to the first 60 s. of the test.

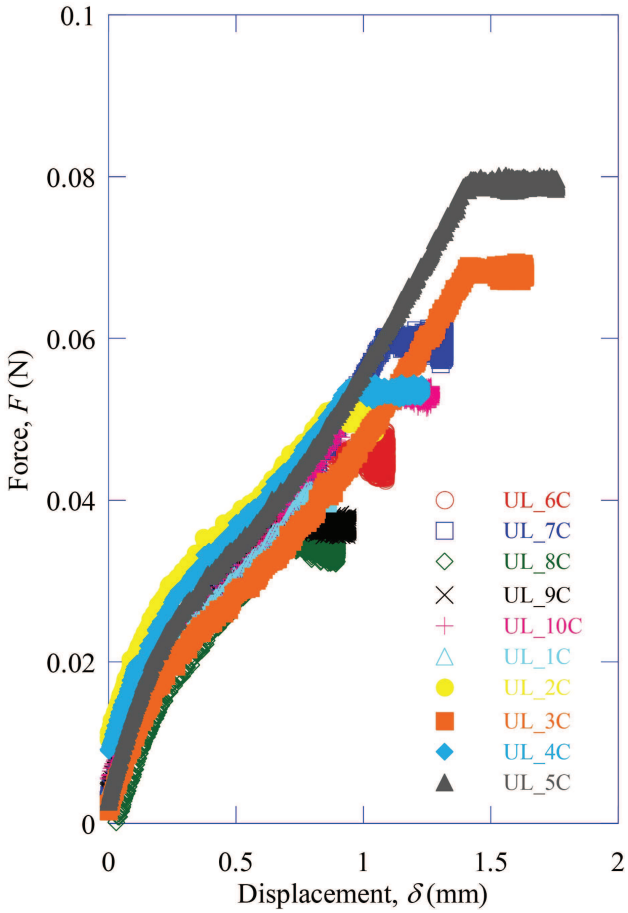

Figure 3.15: Force-displacement creep plot for uniformly loaded fibers up to the first 60 s. of the test.

Table 3.3: Lifetimes of fiber specimens undergoing creep testing.

Sample	Stress (MPa)	Lifetime (s.)
NF_3C	205	618000 (run-out)
NF_4C	279	615000 (run-out)
NF_5C	374	467,965.62
CS_1C	366	29.88
CS_2C	442	40.74
CS_3C	422	26.72
CS_4C	390	20.30
CS_5C	369	40495.90
CS_6C	263	94.94
CS_7C	342	67.06
CS_8C	292	15.86
CS_9C	324	6050.2
CS_10C	354	162.72
UL_1C	417	7.42
UL_2C	521	689780 (run-out)
UL_3C	706	18.92
UL_4C	552	144214.22
UL_5C	818	38.9
UL_6C	470	22870.04
UL_7C	616	1286.5
UL_8C	354	679.52
UL_9C	381	1649.88
UL_10C	548	166.6

The full creep behavior over time is shown in Figure 3.16, Figure 3.17, and Figure 3.18. A few of the individual specimen plots, due to the very large number of data points collected, are graphed with data points sampled at regular intervals for ease of processing. This sampling was not started until after the load-up region had finished and the test had reached its target force.

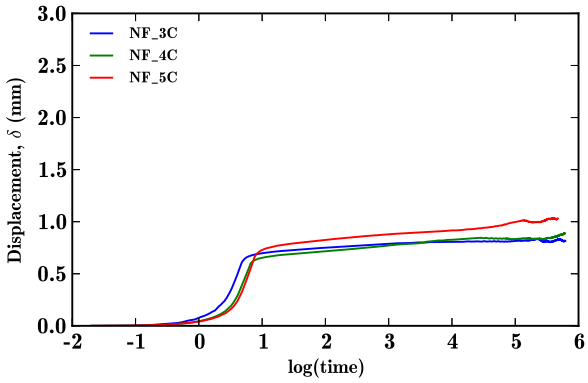

Figure 3.16: Semilog displacement-time creep plot for neat fibers up to failure (or the end of the test). Circles indicate run-outs.

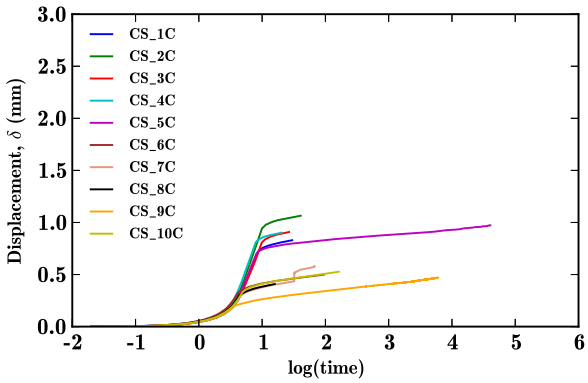

Figure 3.17: Semilog displacement-time creep plot for core-shell fibers up to failure.

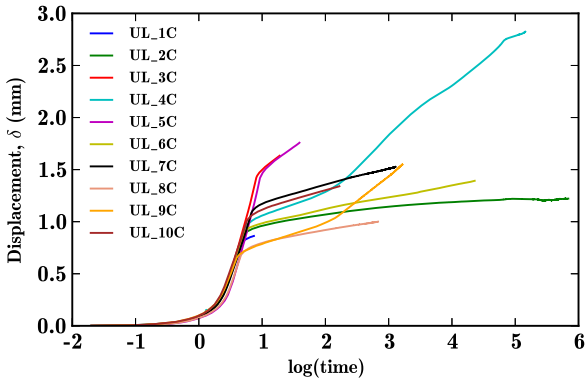

Figure 3.18: Semilog displacement-time creep plot for uniformly loaded fibers up to failure (or the end of the test). Circles indicate run-outs.

In general, all the fibers showed fairly consistent creep behavior over the course of the experiments. After loading up, the fibers experience a period of primary creep in which strain rises rapidly over a short period of time. Afterwards, they settle into a secondary creep stage, slowly accumulating strain at a consistent rate much slower than that seen in the primary creep stage. With the exception of UL_4C and UL_9C, the majority of the fiber specimens experienced no tertiary creep. They either ruptured in the secondary region or continued on in that region past the run-out limit.

3.4 Damage Partitioning

The results obtained from the creep experiments were used to further analyze the fatigue data and determine if cyclic effects contribute heavily to the fibers' failure. The lifetime of a specimen subjected to a static load is given by the following equation[17]:

$$t_f = B\sigma_c^{n-2}\sigma^{-n}\left[1-\left(\frac{\sigma}{\sigma_c}\right)^{n-2}\right], \tag{3.1}$$

where t_f is the lifetime of a creep specimen, B and n are material-specific constants, σ_c is a reference strength (taken as the average tensile strength of the fiber as tested previously), and σ is the stress exerted on the specimen. The values of B and n follow from a setup of two equations with

two unknowns, using the lifetimes of the fiber specimens at two different stress levels as the inputs. This procedure was used to find n for the core-shell and uniformly loaded fibers. The neat fibers featured such long lives at the tested stress level in the creep experiments that it can reasonably be assumed that their lifetimes are dominated primarily by fatigue.

To evaluate n, MATLAB code was written to process the various data points and average the results. Taking the core-shell fibers as an example, there were ten creep specimens tested at a range of stress values below the average tensile strength, yielding ten data points of stress and lifetime. The MATLAB code solved a system of two forms of Equation (3.1) to find n, taking each data point and evaluating it against each of the rest. In this way, the code generated a set of values for n and averaged them into a single constant. In several cases, a comparison of points would result in no solution, but the code accepted this, continued its calculations, and averaged the remaining values.

From the creep data, the lifetime of that same specimen were it subjected to purely cyclic load can be predicted analytically. If that lifetime is greater than the lifetime actually achieved from an experimental fatigue test, this would imply that the experimental specimen suffers from both creep and fatigue. If the calculated lifetime is roughly equal to the lifetime achieved in experiment, this would imply that the cyclic aspect of the fatigue test does not contribute much to the specimen's failure. The equation for determining that lifetime is the following[17]:

$$t_{fc} = g^{-1}\left(\frac{\sigma}{\sigma_m}\right)^n t_f, \tag{3.2}$$

where t_{fc} is the lifetime due purely to cyclic load and σ_m is the midway stress between the mean stress and the amplitude stress. The g term can be computed from[18]

$$g = \Sigma_0^{n/2}\left[\frac{n!}{(n-2l)!(2l)!}\right]\left(\frac{\sigma}{2\sigma_m}\right)^{2l}, \tag{3.3}$$

where l is a whole number index from 0 to the value of $n/2$ rounded up to the nearest whole number. With the lifetimes obtained from experiment and the value of n calculated via Equation (3.1),

Equation (3.2) and Equation (3.3) can be used in conjunction to yield values of t_{fc} corresponding to the ten tests conducted. Carrying out this damage partitioning for the core-shell and uniformly loaded fibers yields the results shown in Figure 3.19 and Figure 3.20, with the predicted values plotted onto the stress-lifetime curves of the corresponding experimental fatigue data. Clearly, there is a wide scatter of theoretical lifetimes in each case, even though a semilog plot of results from Equation (3.2) would initially be expected to produce an approximately linear negative correlation.

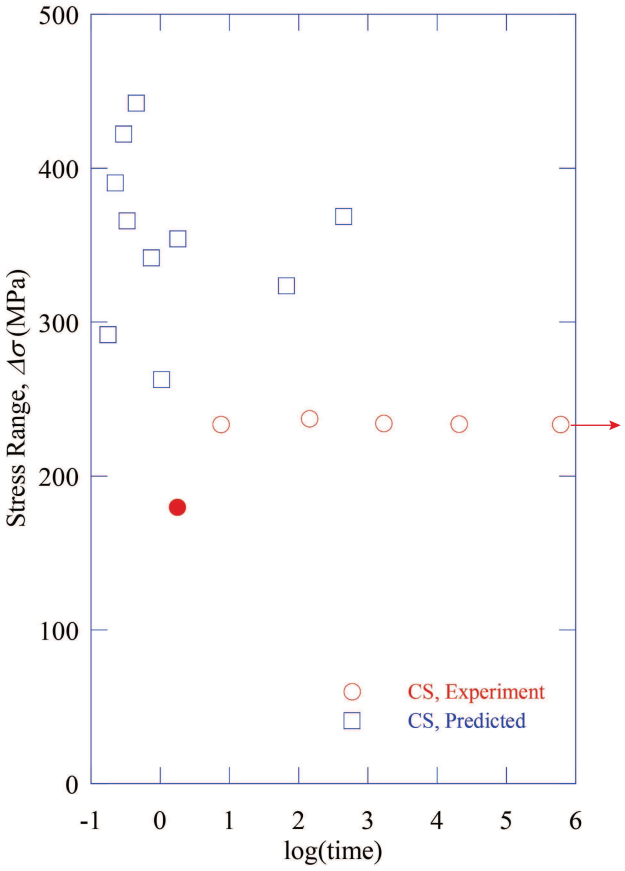

Figure 3.19: Comparison of core-shell fiber predicted cyclic lifetimes and experimental results. Filled-in symbols represent tests that broke in the initial envelope region of the test. Symbols with arrows extending to the right indicate run-out tests.

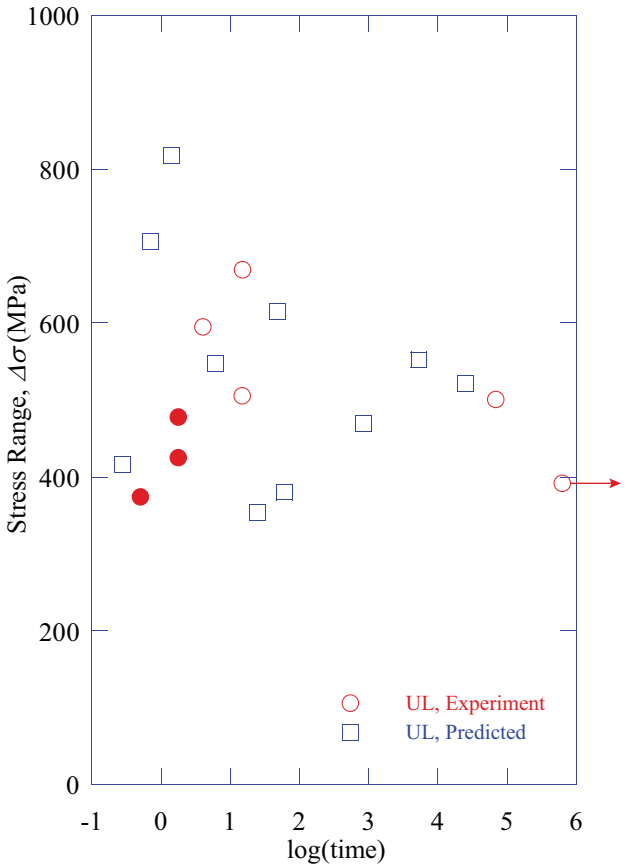

Figure 3.20: Comparison of uniformly loaded fiber predicted cyclic lifetimes and experimental results. Filled-in symbols represent tests that broke in the initial envelope region of the test. Symbols with arrows extending to the right indicate run-out tests.

To understand the reason for the lack of a clear trend, the data from the creep experiments must be examined in terms of strength against time on a log-log plot. Munz et al.[17] notes a strong dependency of constant load lifetimes for ceramics on the applied stress, with an approximately linear negative correlation in the practically useful region of the relationship defined by Equation (3.1). However, as can be seen from Figure 3.21 and Figure 3.22, no such correlation is observed. Thus, the values of t_f obtained experimentally can be expected to skew the results of Equation (3.2) in a way that offers no obvious relationship. To put these results in some perspective, past work has also encountered some difficulties studying creep effects in polyacrylonitrile. For example, Andrews et al.[19] performed creep experiments on polyacrylonitrile films to examine temperature effects and found that the typical S-curve behavior seen in polymers was encountered above the PAN glass

transition temperature, whereas other typical polymers such as polyvinyl chloride (PVC) exhibit such behavior below the glass transition temperature. Increasing stress at a given temperature above the glass transition temperature did feature a progression from flat curves to S-curves, as would be expected, but the lack of a straightforward equivalence of stress and temperature effects, seen in other polymers like PVC, demonstrates the complications in PAN's creep response.

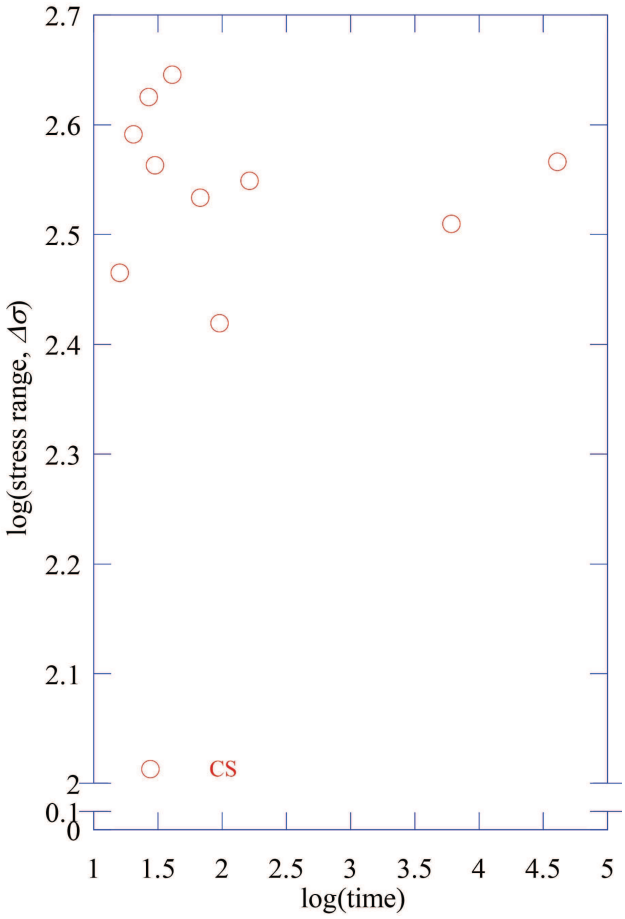

Figure 3.21: Stress-life plot of the core-shell fibers undergoing creep tests expressed on a log-log scale.

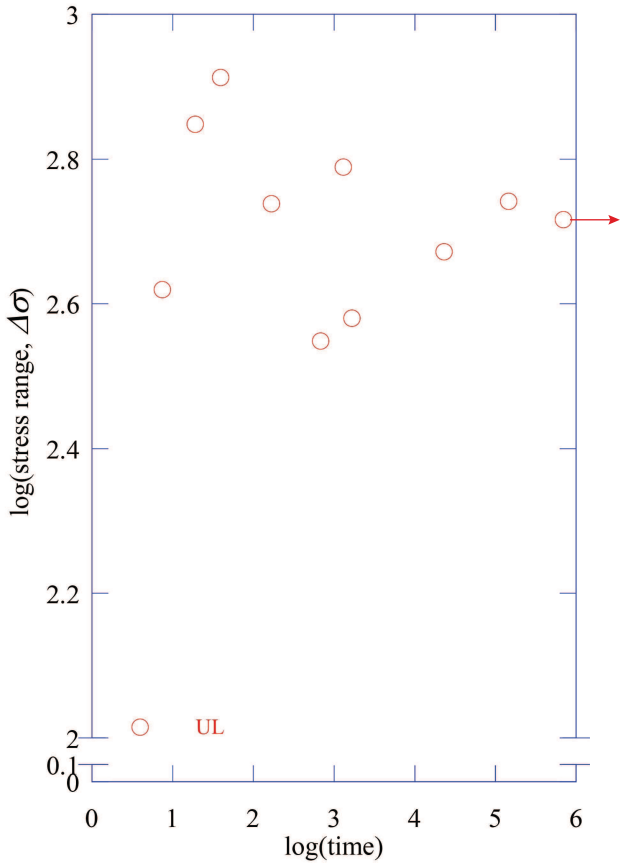

Figure 3.22: Stress-life plot of the uniformly loaded fibers undergoing creep tests expressed on a log-log scale. Symbols with arrows extending to the right indicate run-out tests.

In light of these results, the best that can be achieved is to provide general bounding cases that bracket the outcomes of this analysis. To perform this, two sets of two points were chosen from each set of creep data to produce predictions with the steepest and shallowest negative slopes, with the common point being the test whose amplitude most closely approaches the average tensile strength of the fiber group. The results are shown in Figure 3.23 and Figure 3.24. The wide divergence in the predictions speaks to the wide variability seen in the creep data. The upper bounding line resides above the majority of the experimental values and implies that the predicted cyclic lifetimes of the fibers based solely on static creep data are longer than the cyclic lifetimes observed, signaling a combination of fatigue and creep damage. The lower bounding line, however, resides below those same experimental points and implies the predicted cyclic lifetimes are shorter than

those observed, suggesting that plastic deformation due to creep actually retards damage accumulation due to fatigue. Such a wide scatter raises the question of whether the damage accumulation processes are varying from specimen to specimen, as the internal structure of polymers can exhibit large variation. Answering this question would require the difficult tasks of monitoring crack initiation and propagation within the specimens. Given various factors such as the fibers' small diameter and non-uniformity both along the length and across the cross-section, achieving the goal of reliably confirming the method (or methods) of damage accumulation would be quite arduous. What does appear clear from the results is that this method of damage partitioning is an inaccurate way to process the data. Creep and fatigue are clear and present factors that do interact in these systems, but treating them as additive mechanisms of damage is not valid.

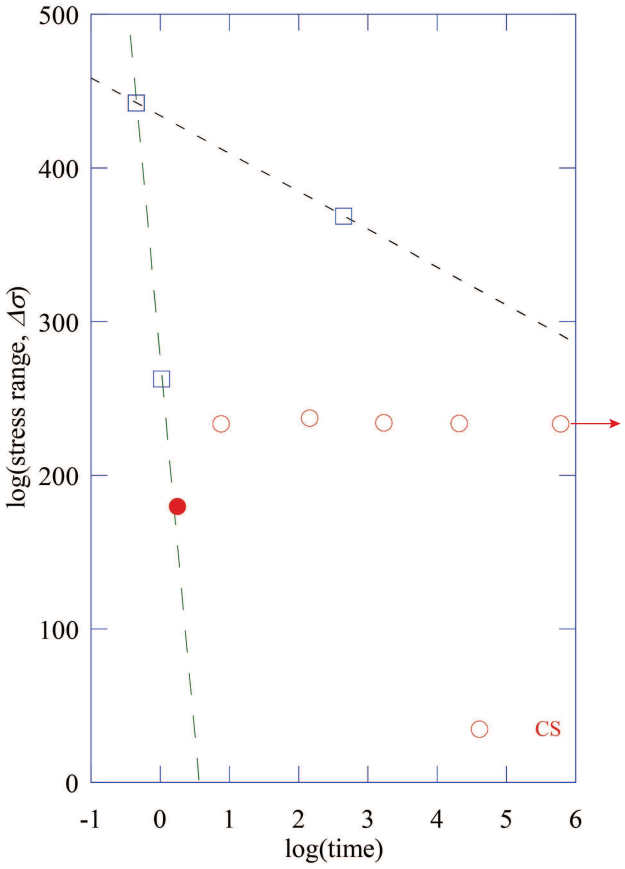

Figure 3.23: Stress-life plot of the core-shell fibers under cyclic loading, with predicted bounding cases. Filled in symbols represent specimens that failed prior to reaching the target amplitude. Symbols with arrows extending to the right indicate run-out tests.

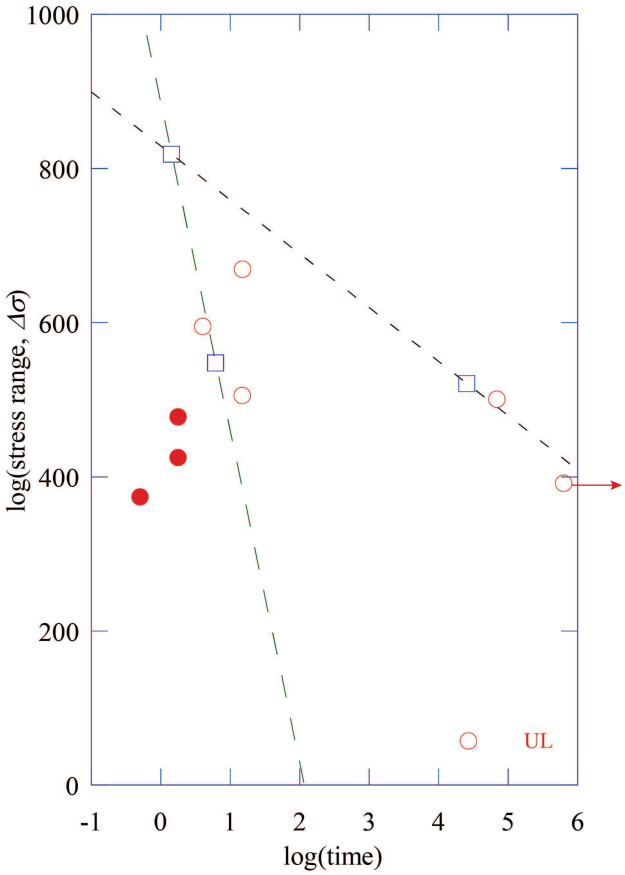

Figure 3.24: Stress-life plot of the uniformly loaded fibers under cyclic loading, with predicted bounding cases. Filled in symbols represent specimens that failed prior to reaching the target amplitude. Symbols with arrows extending to the right indicate run-out tests.

3.5 Fractography

Fracture images of ruptured fiber specimens were taken after completion of the mechanical tests. Tensile fracture surfaces are provided for the core-shell and neat fiber. For the fatigue and creep experiments, fracture images for short and long lifetimes that produced fracture surfaces were taken for each of the three fiber sets. What follows is a sequence of scanning electron micrographs displaying fracture surfaces for each fiber group after each type of experiment. Tensile surfaces are shown in Figure 3.25, Figure 3.26, and Figure 3.27. Fatigue surfaces are shown from Figure 3.28 to Figure 3.33. The last five figures, from Figure 3.34 to Figure 3.38, display creep surfaces. Out of three neat fiber tests, only one produced a break, and that only occurred after five days of testing.

Thus, it is presented as the only neat fiber creep fracture.

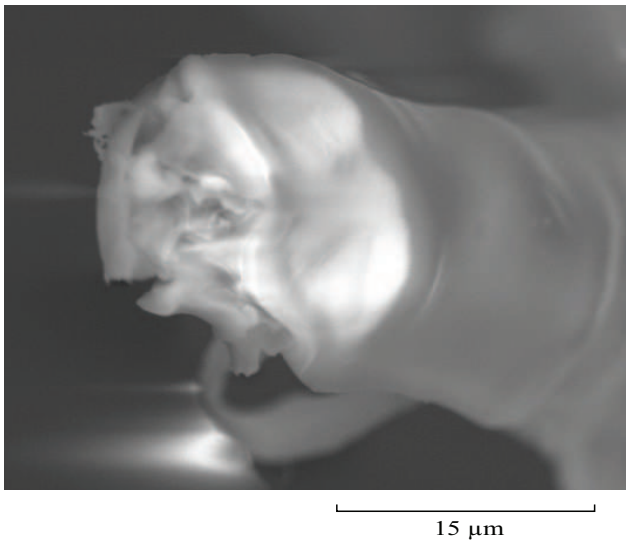

Figure 3.25: Neat fiber tensile fracture for NF_11T (σ_f=508 MPa).

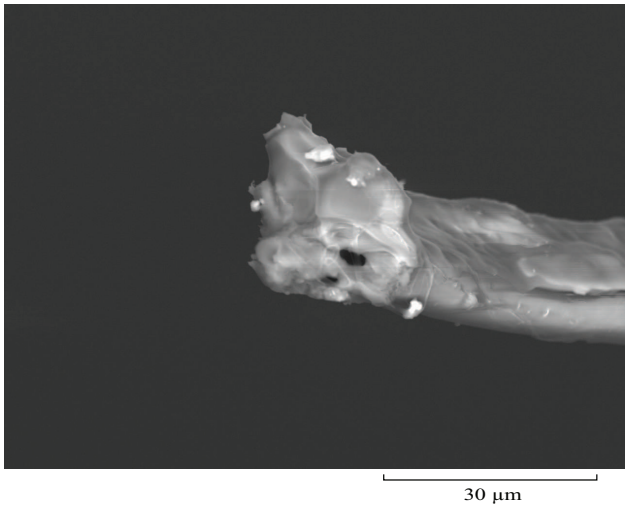

Figure 3.26: Core-shell fiber tensile fracture for CS_3T (σ_f=659 MPa).

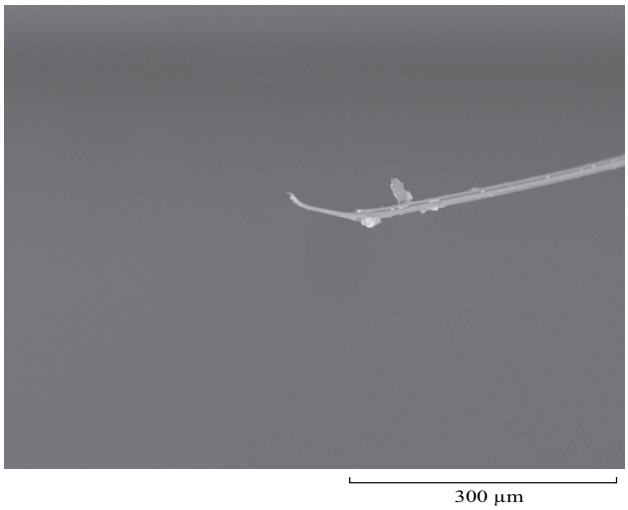

Figure 3.27: Uniformly loaded fiber tensile fracture for UL_1T (σ_f=1030 MPa).

Immediately apparent is that the uniformly loaded tensile failure is easy to distinguish from the failures of the other two. The fragment of fiber extending from the fracture surface of UL_1T is indicative of an axial split accompanying multiple granular breaks, a feature seen in Courtelle acrylic fibers.[20] Meanwhile, the NF_11T and CS_3T specimens display uneven surfaces and irregular edges but generally do not feature the grainy texture of a typical granular break seen in other acrylic fracture surfaces. This may be indicative of a more ductile fracture mechanism, which is commonly seen in polymers such as nylon and polypropylene, although triacetate has shown a granular fracture mechanism that results in a smoother surface than a typical granular break.[20]

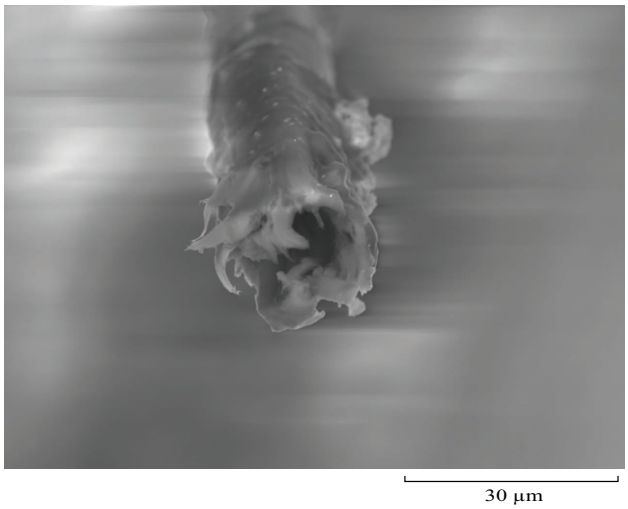

Figure 3.28: Neat fiber fatigue fracture for NF_10F ($\Delta\sigma$=304 MPa, long lifetime=27822 cycles).

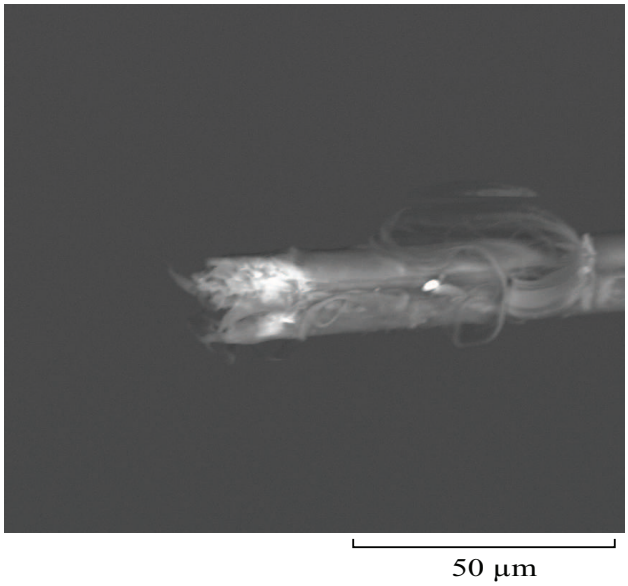

Figure 3.29: Neat fiber fatigue fracture for NF_9F ($\Delta\sigma$=358 MPa, short lifetime=58 cycles).

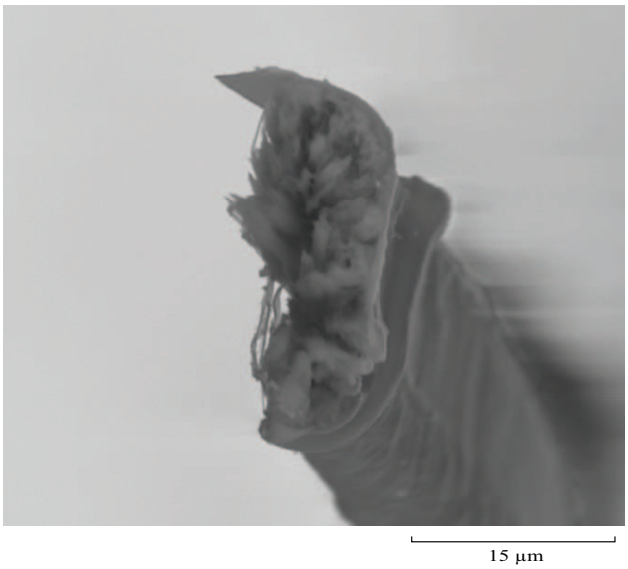

Figure 3.30: Core-shell fiber fatigue fracture for CS_8F ($\Delta\sigma$=260 MPa, long lifetime=20538 cycles).

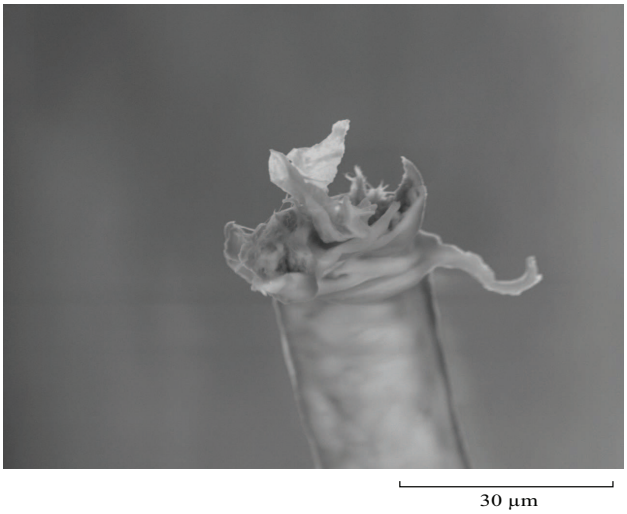

Figure 3.31: Core-shell fiber fatigue fracture for CS_9F ($\Delta\sigma$=203 MPa, short lifetime=2 cycles).

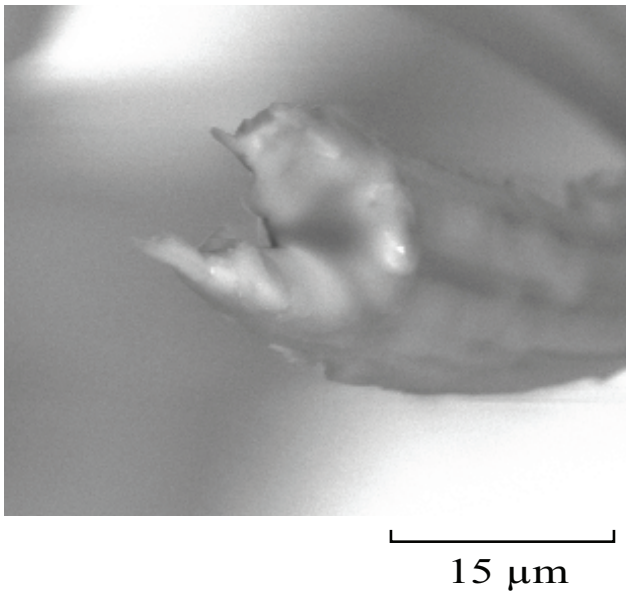

Figure 3.32: Uniformly loaded fiber fatigue fracture for UL_15F ($\Delta\sigma$=557 MPa, long lifetime=67635 cycles).

Figure 3.33: Uniformly loaded fiber fatigue fracture for UL_11F ($\Delta\sigma$=545 MPa, short lifetime=2 cycles).

Comparing the images, there is no obvious difference between long and short lifetimes for each fiber under the fatigue loading condition. The neat and core-shell fibers, to varying degrees, seem to show granular fracture surfaces in which the "granules" appear to be elongated projections.[20] This is a mechanism seen in tensile breaks of polyvinyl alcohol.[20] The uniformly loaded fiber surfaces are largely lacking in distinguishing features, perhaps another example of the smoother granular fracture surface seen in triacetate.[20]

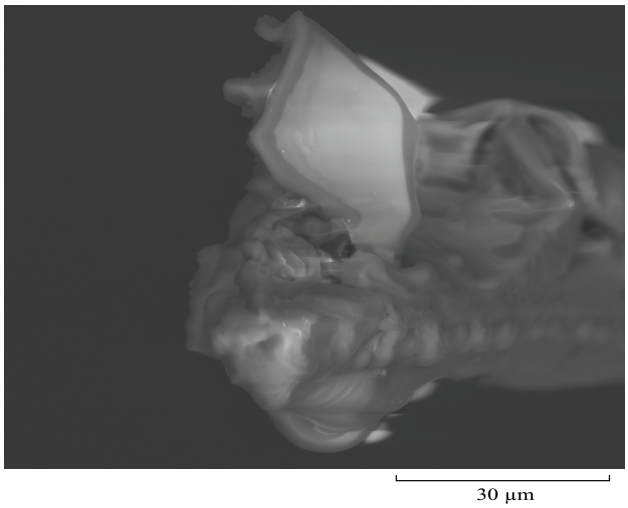

Figure 3.34: Neat fiber creep fracture for NF_5C (σ=374 MPa, long lifetime=467965 s.).

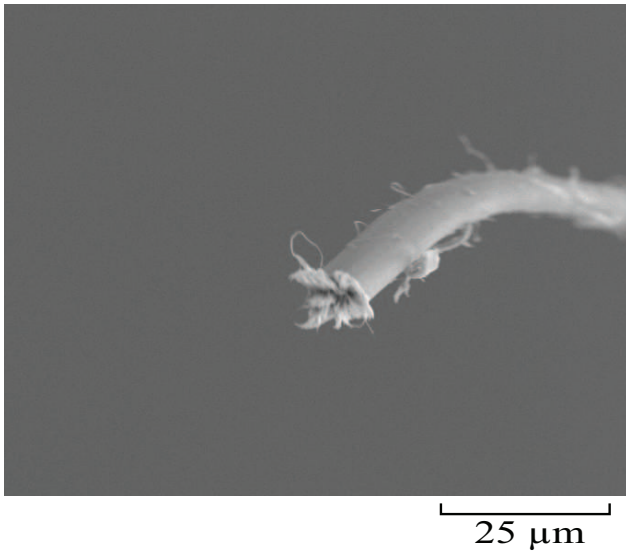

Figure 3.35: Core-shell fiber creep fracture for CS_9C (σ=324 MPa, long lifetime=6051 s.).

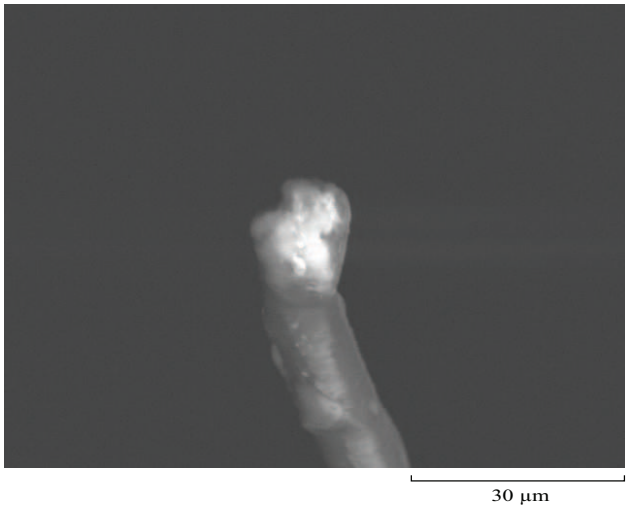

Figure 3.36: Core-shell fiber creep fracture for CS_4C (σ=390 MPa, short lifetime=20.30 s.).

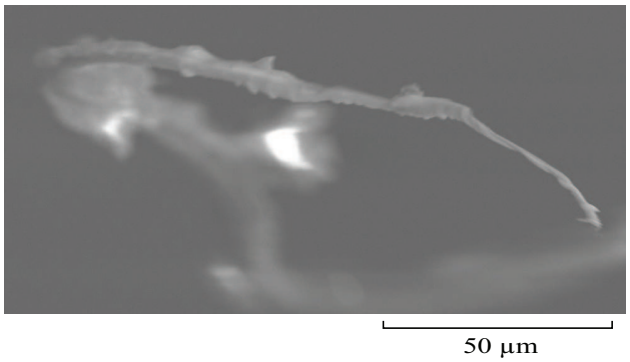

Figure 3.37: Uniformly loaded fiber creep fracture for UL_6C (σ=470 MPa, long lifetime=22871 s.).

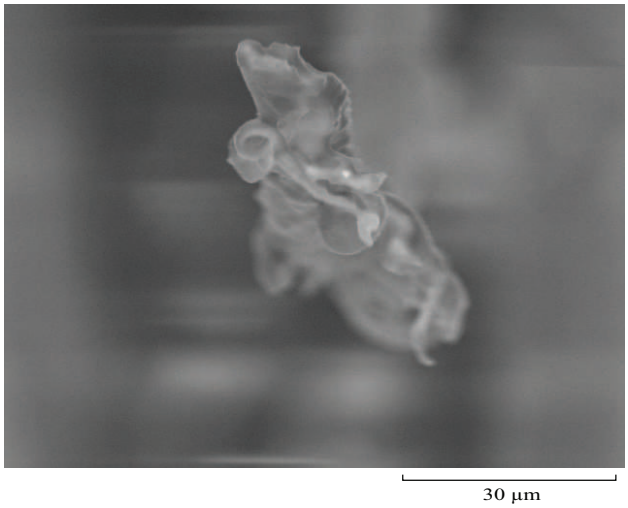

Figure 3.38: Uniformly loaded fiber creep fracture for UL_1C (σ=417 MPa, short lifetime=8 s.).

The unusual appearance of the neat fiber creep fracture surface, once taking the length scale into account, probably implies that outside materials have adhered to the end of the fiber fragment. Assuming the lighter-colored area in the lower left-hand corner of the imaged structure is the fiber surface, there does not appear to be an abundance of features, so it is possibly another smooth granular surface. Both the long and short lifetime uniformly loaded fiber specimens appear to have tails trailing off the ends, resembling the uniformly loaded tensile break. Meanwhile, unlike the fatigue tests, there is more to distinguish between the long and short lifetimes of the core-

shell fibers. The long lifetime surface has the appearance of elongated projections, while the short lifetime surface has the appearance of the smooth granular surface. Unfortunately, there is not an abundance of creep fracture surfaces to compare against in the literature, but all the observed surfaces have been seen before in one form or another.

Overall, fracture surfaces appeared to vary somewhat by loading condition. Neat fibers produced a smoother surface in tensile loading but more ragged features in fatigue loading. The same can be said for the core-shell fibers, and additionally, the longer lifetime creep surface bore more resemblance to the fatigue surfaces while the shorter lifetime creep surface resembled the tensile surface. Finally, the uniformly loaded tensile and creep surfaces both featured the same combination of granular fractures and axial splitting, which distinguished them from the smoother fatigue surfaces for that fiber group.

4 Conclusions

Tensile, fatigue, and creep experiments were conducted on three different configurations of PAN based single fibers. The neat fibers displayed a mean failure stress value of 591 $\pm$ 159 MPa, the core-shell fibers yielded a mean failure stress of 527 $\pm$ 125 MPa, and the uniformly loaded fibers exhibited a mean failure stress of 697 $\pm$ 186 MPa. Meanwhile, all of the fiber groups clearly experienced cyclic fatigue damage. The neat fibers' shortest lifetime ran 2.75 cycles, and the longest lifetime was a run-out after over 601,000 cycles. The core-shell fibers' shortest lifetime ran 1.75 cycles, and the longest lifetime was a run-out after over 601,000 cycles. The uniformly loaded fibers' shortest lifetime ran 0.5 cycle, and the longest lifetime was a run-out after over 619,000 cycles.

Greater variability among the three fiber groups was observed during the creep experiments. While the neat fibers displayed very long creep lifetimes lasting multiple days, the core-shell specimens all ruptured within a single day at a variety of stress amplitudes, with lifetimes ranging from about 16 s. to 40,500 s. The uniformly loaded fibers, meanwhile, varied in creep lifetime from about 8 s. to a run-out of about 690,000 s. While creep is clearly observed in the loaded fibers, its exact relationship with stress level is unclear as there is no obvious relationship between creep life and applied amplitude. Attempts to partition the damage sustained by the loaded fibers did not produce any clear correlation between creep life and pure fatigue life, and the best that can be done is the establishment of bounding cases to define the range of possible results. This indicates that trying to separate creep and fatigue into distinct contributions is not a valid method for characterizing damage accumulation in these fiber systems.

Overall, all three fiber groups display the effects of cyclic and time dependent damage accumulation, but their individual responses to these mechanisms vary widely. The most concrete example of this can be seen from the significantly higher creep failure susceptibility experienced by the loaded fiber configurations. It is clear that the different processing histories and morphologies characterizing each fiber group play prominent roles in how the fatigue and creep processes inter-

act to cause failure. The relationship between fatigue and creep in these systems is more complex than what can be simply defined by a partitioning scheme, and more research into that relationship is crucial in order to completely define the damage accumulation occurring in the fibers.

Bibliography

[1] R. Jain, M. L. Minus, H. G. Chae, S. Kumar, Processing, structure, and properties of pan/mwnt composite fibers, Macromolecular Materials and Engineering 295 (8) (2010) 742–749.

[2] A. R. Bunsell, T. I. M. England), Handbook of tensile properties of textile and technical fibres, / edited by A.R. Bunsell. ill. "The Textile Institute." Includes bibliographical references and index. Access is available to the Yale community. Woodhead publishing in textiles ; no. 91. Yale Internet Resource None Online resource (2009).

[3] H. G. Chae, T. V. Sreekumar, T. Uchida, S. Kumar, A comparison of reinforcement efficiency of various types of carbon nanotubes in poly acrylonitrile fiber, Polymer 46 (24) (2005) 10925–10935.

[4] H. G. Chae, M. L. Minus, S. Kumar, Oriented and exfoliated single wall carbon nanotubes in polyacrylonitrile, Polymer 47 (10) (2006) 3494–3504.

[5] S. Suresh, Fatigue of materials, Cambridge solid state science series, Cambridge University Press, Cambridge England ; New York, 1991, 91009213 (Subra) S. Suresh. ill. ; 23 cm. Includes bibliographical references (p. [518]-562) and indexes.

[6] A. R. Bunsell, J. W. S. Hearle, R. D. Hunter, Apparatus for fatigue-testing of fibres, Journal of Physics E-Scientific Instruments 4 (11) (1971) 868–872.

[7] A. R. Bunsell, J. W. S. Hearle, Fatigue of synthetic polymeric fibers, Journal of Applied Polymer Science 18 (1) (1974) 267–291.

[8] A. R. Bunsell, J. W. S. Hearle, Konopase.L, B. Lomas, Preliminary study of fracture morphology of acrylic fibers, Journal of Applied Polymer Science 18 (8) (1974) 2229–2242.

[9] J. A. Bencomo-Cisneros, A. Tejeda-Ochoa, J. A. Garcia-Estrada, C. A. Herrera-Ramirez, A. Hurtado-Macias, R. Martinez-Sanchez, J. M. Herrera-Ramirez, Characterization of kevlar-29 fibers by tensile tests and nanoindentation, Journal of Alloys and Compounds 536 (2012) S456–S459.

[10] O. Harzallah, H. Benzina, J. Y. Drean, Physical and mechanical properties of cotton fibers:

Single-fiber failure, Textile Research Journal 80 (11) (2010) 1093–1102.

[11] P. Davies, A. R. Bunsell, E. Chailleux, Tensile fatigue behaviour of pbo fibres, Journal of Materials Science 45 (23) (2010) 6395–6400.

[12] C. Lechat, A. R. Bunsell, P. Davies, Tensile and creep behaviour of polyethylene terephthalate and polyethylene naphthalate fibres, Journal of Materials Science 46 (2) (2011) 528–533.

[13] H. Mahfuz, A. Adnan, V. K. Rangari, M. M. Hasan, S. Jeelani, W. J. Wright, S. J. DeTeresa, Enhancement of strength and stiffness of nylon 6 filaments through carbon nanotubes reinforcement, Applied Physics Letters 88 (8) (2006) 083119-1–083119-3.

[14] E. M. Moore, D. L. Ortiz, V. T. Marla, R. L. Shambaugh, B. P. Grady, Enhancing the strength of polypropylene fibers with carbon nanotubes, Journal of Applied Polymer Science 93 (6) (2004) 2926–2933.

[15] V. K. Rangari, M. Y. Shaik, H. Mahfuz, S. Jeelani, Fabrication and characterization of high strength nylon-6/si3n4 polymer nanocomposite fibers, Materials Science and Engineering a-Structural Materials Properties Microstructure and Processing 500 (1-2) (2009) 92–97.

[16] V. K. Rangari, Y. M. Shaik, G. M. Mohammad, S. Jeelani, Reinforcement of si3n4 nanoparticles in polypropylene single fibers through melt extrusion process and their properties, Journal of Applied Polymer Science 121 (3) (2011) 1512–1520.

[17] D. Munz, T. Fett, Ceramics : mechanical properties, failure behaviour, materials selection, Springer series in materials science, Springer, Berlin ; New York, 1999, 99010778 Dietrich Munz, Theo Fett. ill. ; 24 cm. Includes bibliographical references and index.

[18] A. G. Evans, E. R. Fuller, Crack-propagation in ceramic materials under cyclic loading conditions, Metallurgical Transactions 5 (1) (1974) 27–33.

[19] R. D. Andrews, H. Okuyama, Rheo-optical behavior of polyacrylonitrile - creep and creep recovery, Journal of Applied Physics 39 (11) (1968) 4909–4914.

[20] J. W. S. Hearle, Fibre failure and wear of materials : an atlas of fracture, fatigue, and durability, Ellis Horwood series in polymer science and technology, Ellis Horwood ; Halsted Press, Chichester, England New York, 1989, 89015211 Â£58.00 J.W.S. Hearle ... [et al.]. ill. ; 25 cm. Includes index. Bibliography: p. [443]-449.